

**AN INVESTIGATION OF AIRFLOW OVER THE AFT  
PORTIONS OF A VARIABLE SWEEP FIGHTER CONFIGURATION**

**By**

**Ernald B. Graves**

**Bachelor of Science in Mechanical Engineering (Aero Option),  
University of Pittsburgh  
1967**

**A thesis submitted to  
the Faculty of  
The School of Engineering and Applied Science  
of the George Washington University in partial fulfillment  
of the requirements for the degree of**

**MASTER OF SCIENCE**

**(NASA-CR-146361) AN INVESTIGATION OF  
AIRFLOW OVER THE AFT PORTIONS OF A VARIABLE  
SWEEP FIGHTER CONFIGURATION M.S. Thesis  
(George Washington Univ.) 74 p HC \$4.50**

**N76-17022**

**Unclass**

**CSCL 01: G3/02 13314**

**December 1975**

**NASA STI FACILITY  
INPUT BRANCH**

## ABSTRACT

An investigation of airflow over the aft portions of a variable sweep fighter aircraft configuration has been performed. Tests conducted in the Langley Unitary Plan wind tunnel at Mach number 2.16 included measurements of forces, moments, and local static pressures as well as visual recordings of the airflow. An aerodynamic analytical prediction method was evaluated when used in data comparison at angles of attack of 0, 5, and 15 degrees.

The results of this investigation indicate that in supersonic flow the typical outboard located twin vertical tail arrangement tends to provide a more positive increment in normal-force on the afterbody fuselage and the horizontal tail than a single center-mounted vertical tail of similar planform shape. In addition, the results indicate that a method for aerodynamic analysis of wing-body-tail configurations currently available at Langley Research Center can provide reasonable estimates of pressure coefficient distributions on configurations in regions of complex supersonic flow. At this time, however, the available analytical method cannot adequately replace experimental wind tunnel tests for determining the supersonic flow environment of a given configuration. Experimental flow visualization techniques, in particular, can provide data significant to the improvement of aerodynamic analytical predictions methods.

## ACKNOWLEDGEMENTS

The author wishes to express his appreciation to the National Aeronautics and Space Administration for providing through its graduate studies program, the opportunity to perform this research and prepare this thesis.

Special gratitude is extended to those many individuals whose efforts have contributed to the completion of this thesis in a timely manner.

## TABLE OF CONTENTS

	Page
TITLE .....	i
ABSTRACT .....	ii
ACKNOWLEDGEMENTS .....	iii
TABLE OF CONTENTS .....	iv
LIST OF SYMBOLS .....	v
LIST OF TABLES .....	vii
LIST OF FIGURES .....	viii
Chapter	
I. INTRODUCTION .....	1
II. EXPERIMENTAL APPARATUS AND PROCEDURE .....	3
III. ANALYTICAL METHOD .....	14
IV. RESULTS AND DISCUSSION .....	19
V. CONCLUDING REMARKS .....	52
REFERENCES .....	54
APPENDIX .....	56



## LIST OF SYMBOLS

$b$	span, .402 m
$\bar{c}$	reference chord, .243 m
$C_D$	drag coefficient, $\frac{\text{drag}}{qS}$
$C_m$	pitching moment coefficient, $\frac{\text{pitching moment}}{qS\bar{c}}$
$C_N$	normal force coefficient, $\frac{\text{normal force}}{qS}$
$C_p$	pressure coefficient, $\frac{p_\ell - p_\infty}{q}$
$\Delta C_p$	$C_{p,u} - C_{p,\ell}$
$C_{p,u}$	upper surface pressure coefficient
$C_{p,\ell}$	lower surface pressure coefficient
$\ell$	fuselage length, .783 m
$L/D$	lift-drag ratio
$p_\ell$	local static pressure
$p_\infty$	free stream static pressure
$q$	free stream dynamic pressure
$S$	reference area, .113 m <sup>2</sup>

$x/c$	fraction of local chord
$x/l$ or $x/\ell$	fraction of fuselage length
$y/b'$	fraction of local span (horizontal)
$z/b'$	fraction of local span (vertical)
$\alpha$	angle of attack, degrees
$\gamma$	ratio of specific heats

## LIST OF TABLES

Table	Page
1. AFT FUSELAGE ORIFICE LOCATIONS .....	10
2. TAIL SURFACE ORIFICE LOCATIONS .....	10
3. COMPARISON OF FORCE AND PRESSURE RESULTS ON NORMAL FORCE COEFFICIENT DUE TO HORIZONTAL AND SINGLE VERTICAL TAILS .....	36
4. COMPARISON OF SOME AERODYNAMIC RESULTS FROM FORCE TESTS WITH ANALYTICAL PREDICTIONS .....	49
5. ANALYTICAL METHOD COMPUTATIONAL DATA .....	50

## LIST OF FIGURES

Figure	Page
1. Sketch of the Langley Unitary Plan wind tunnel arrangement .....	5
2. Photographs of models installed in the Langley Unitary Plan wind tunnel .....	7
3. Drawing of the model .....	8
4. Representation of the analytical model .....	11
5. Distribution of pressure coefficients on the afterbody fuselage without the presence of tails .....	20
6. Comparison of pressure coefficient distributions on the afterbody fuselage with various tail arrangements .....	22
7. Comparison of pressure coefficient distributions on the starboard surface of various vertical tails .....	26
8. Comparison of pressure coefficient distributions on the port and starboard surfaces of the twin vertical tail .....	27
9. Distribution of pressure coefficients on the upper and lower surfaces of the horizontal tail in the presence of the single vertical tail .....	28
10. Comparison of pressure coefficient distributions on the horizontal tail for various vertical tail arrangements .....	29
11. Vapor screen photographs of the model at an angle-of-attack of 15 degrees.....	32
12. Schlieren photographs of the model with various tail arrangements .....	34
13. Longitudinal aerodynamic characteristics of the model .....	37
14. Distribution of net pressure coefficients on the afterbody fuselage with various tail arrangements .....	39

Figure	Page
15. Distribution of net pressure coefficients on the horizontal tail for various vertical tail arrangements .....	42
16. Distribution of net isobars on the horizontal tail in the presence of the single vertical tail .....	43
17. Comparison of analytical predictions with experimental pressure data on the afterbody fuselage .....	45
18. Comparison of analytical predictions with experimental pressure data on the horizontal tail .....	46
19. Comparison of spanwise distribution of net pressure coefficients from experimental data on the horizontal tail with analytical predictions .....	48

## CHAPTER I

### INTRODUCTION

The National Aeronautics and Space Administration maintains a continuous effort to assess the future needs of the United States in such areas as aeronautical research and development. Recent assessments have led to the prediction that in the 1980's, fighter aircraft will be sought by the military that can simultaneously sustain supersonic flight and high maneuverability.

Of significant importance in the design and development of aircraft has been the availability of analytical methods to predict the airflow distribution (aerodynamic characteristics) for a given configuration. These methods have been quite useful as a design and evaluation tool for aircraft in subsonic flow and at small incidence angles. Valid analytical results have also been obtained in the supersonic flow environment for aerodynamically refined cruise aircraft at small angular incidences. But unlike the low incidences encountered by a supersonic cruise aircraft, highly maneuverable aircraft such as those used for defense purposes will encounter large incidence angles. It is under these conditions of supersonic flow and large incidence that classical flow theories become invalid. Complex flow regions where strong shocks, large vorticity gradients, and flow separation are likely to occur are located downstream of the wing where the surfaces used for aircraft

stability and control are located. For lack of a more reliable approach, solutions to these types of problems have been treated by extensive and time consuming experimental studies.

The present investigation was conducted to provide a technology base to promote a better understanding of the complex flow in the region about the afterbody fuselage. Emphasis was focused on providing a consistent set of experimental data that could be used to improve or develop new techniques for predicting aircraft flow distribution and resultant loads. Comparison of experimental and analytical data has been made at Mach number 2.16 and an aerodynamic analytical prediction method evaluated. The test configuration is representative of a combat fighter aircraft and analysis is conducted at angles-of-attack of about 0, 5, and 15 degrees.

# CHAPTER II

## EXPERIMENTAL APPARATUS AND PROCEDURE









### General Procedure

A variable sweep fighter aircraft configuration was investigated in the Langley Unitary Plan wind tunnel to determine aerodynamic forces and moments in addition to airflow distribution on the aft fuselage and tail surfaces. Experiments were conducted at the following constant conditions:

Mach number ----- 2.16  
 Reynolds number, per meter -----  $6.56 \times 10^6$   
 Stagnation pressure,  $N/m^2$  ----- 64 590.47  
 Stagnation temperature, °K ----- 324.82  
 $\gamma$ , air ----- 1.4

Boundary layer transition strips were affixed on the model nose, inlet wedge, and all airfoil surfaces in accordance with references 1 and 2.

The configuration matrix chart below depicts the configuration tail positions for various studies.

Pressure	Force	Analytical
		
		
		
		



## Wind Tunnel

This investigation was conducted in the low Mach number test section of the Langley Unitary Plan wind tunnel. The wind tunnel is a closed-loop, variable-pressure facility that uses an asymmetric sliding-block type nozzle in each test section which permits : continuous variation in Mach number from about 1.5 to 2.9 in the low Mach number test section and from about 2.3 to 4.7 in the high Mach number test section. Each test section is about 1.22 meters square and about 2.13 meters long. A schematic drawing of the tunnel arrangement is presented in figure 1.

## Model

General - The general configuration is representative of current day variable sweep fighter aircraft. The inlets that would exist on an actual aircraft were modified to facilitate experimental and analytical methods. The configuration modification consisted of wedge shaped inlet extensions upstream of the simulated ducts. The wedge was designed in accordance with reference 3 to assure attached shocks at the wedge leading edge through the test angle of attack range at the Mach number of 2.16.

The "pressure" and "force" models tested in this investigation used a common forebody. The aft fuselage, horizontal tails and vertical tails were geometrically similar for both the "force model" and "pressure model". All tails were NACA 65A004 airfoils. Both models were rigidly

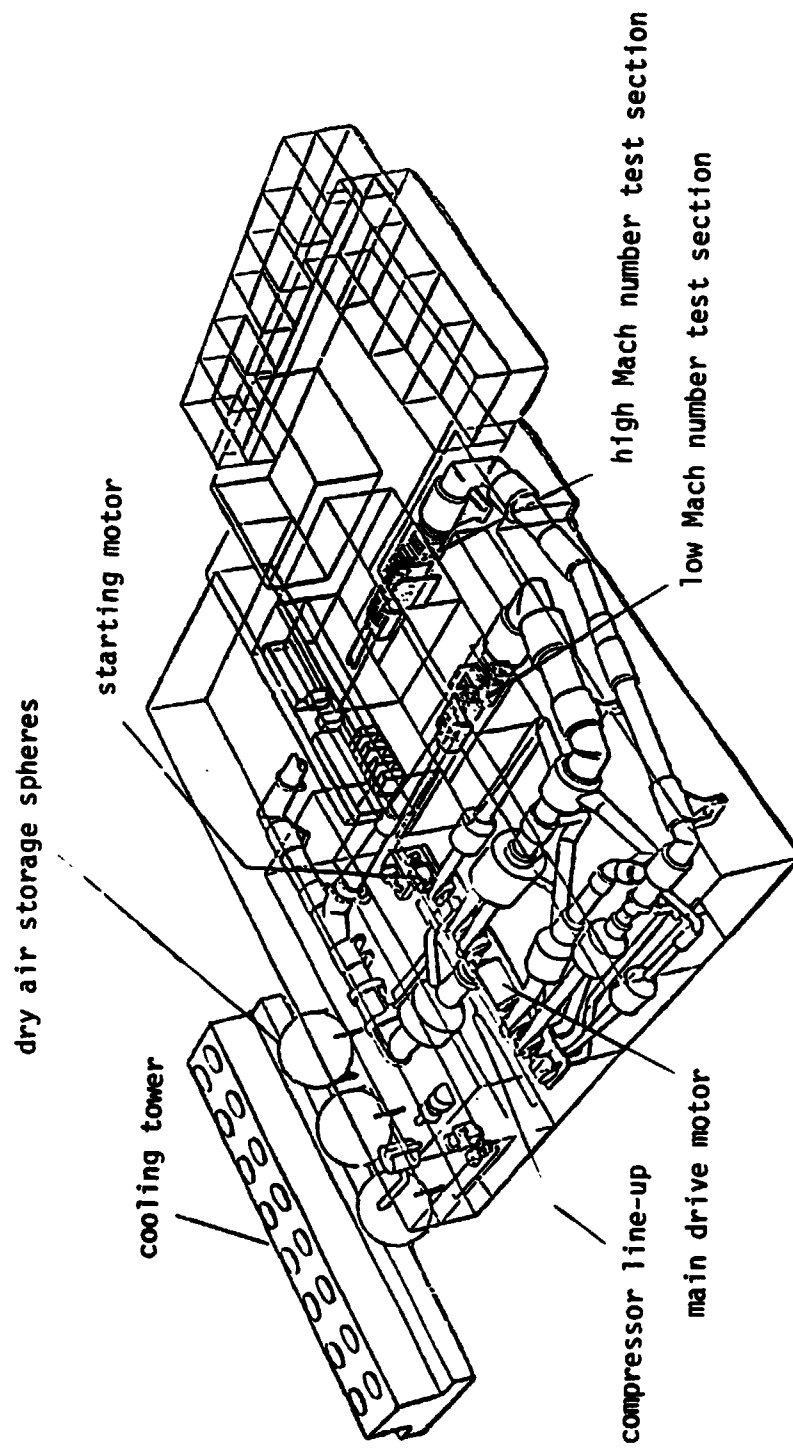


Figure 1. - Sketch of the Langley Unitary Plan wind tunnel arrangement.

attached to the tunnel sting support system. Figure 2 shows photographs of the pressure and force models mounted in the test section. Figure 3 shows a general sketch of the models.

Pressure model. - The aft fuselage and tail surfaces incorporated static pressure orifices. The tails were formed by an integral casting technique described in reference 4. The aft fuselage was made of machined aluminium. Orifice tubing for the fuselage was exited at the fuselage base. Since orifice tubing for the tail surfaces was channeled thru the engine ducts, to avoid the detached shock conditions that would have occurred due to blockage in the duct the inlets were wedged as has been previously mentioned.

The orifice locations on the fuselage were spaced as described in Table 1. A single center-line mounted vertical tail or a twin-outboard vertical tail arrangement could be installed. The model had horizontal tails essentially in-line with the wing. The left horizontal tail was not instrumented. The orifice locations for the tail surfaces were systematically arranged as shown in figure 3 (b) and described in Table 2.

Force model. - The model used for force tests is sketched in figure 3 (a). The single center vertical tail and horizontal tails could be removed. All model parts were of machined aluminium.

Analytical model. - The geometrical representation of the analytical model is displayed in figure 4. Shown is a computer generated drawing of the primary test configuration with the single vertical tail.

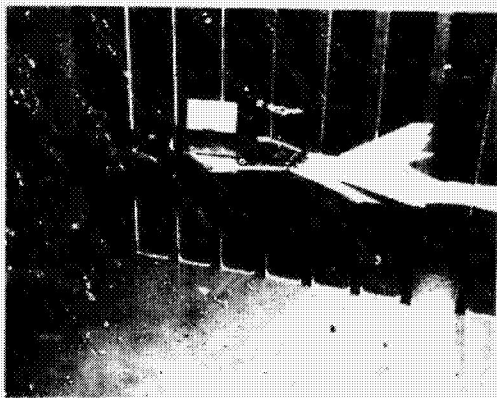
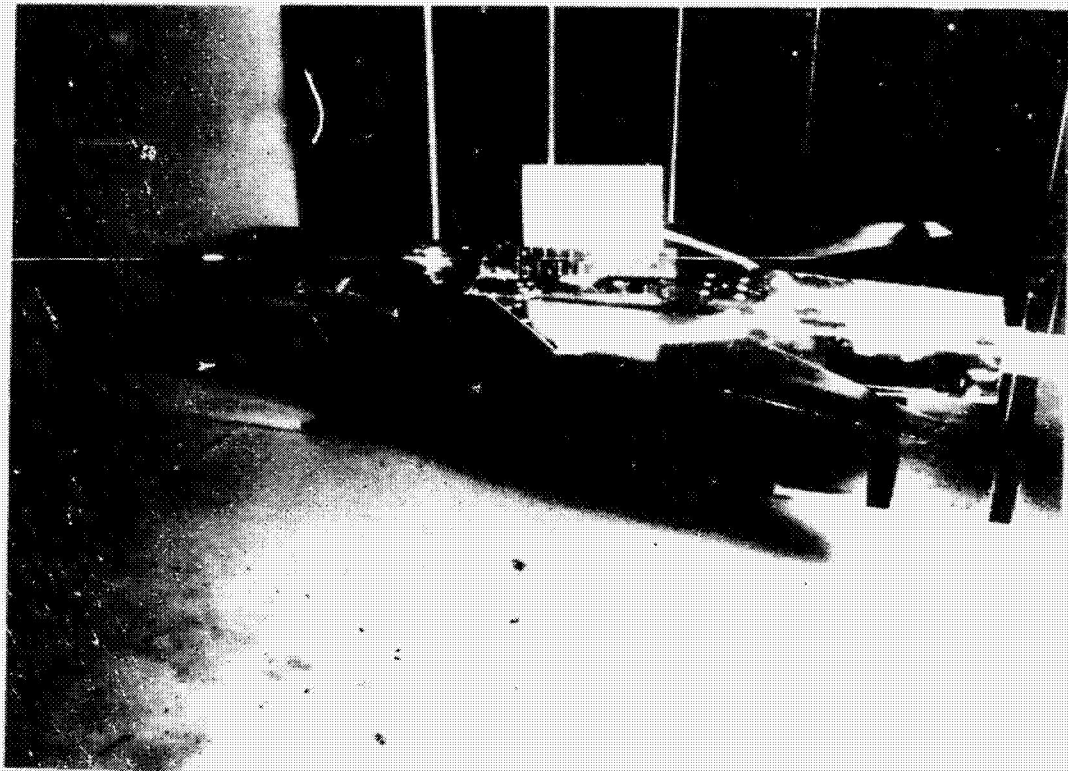
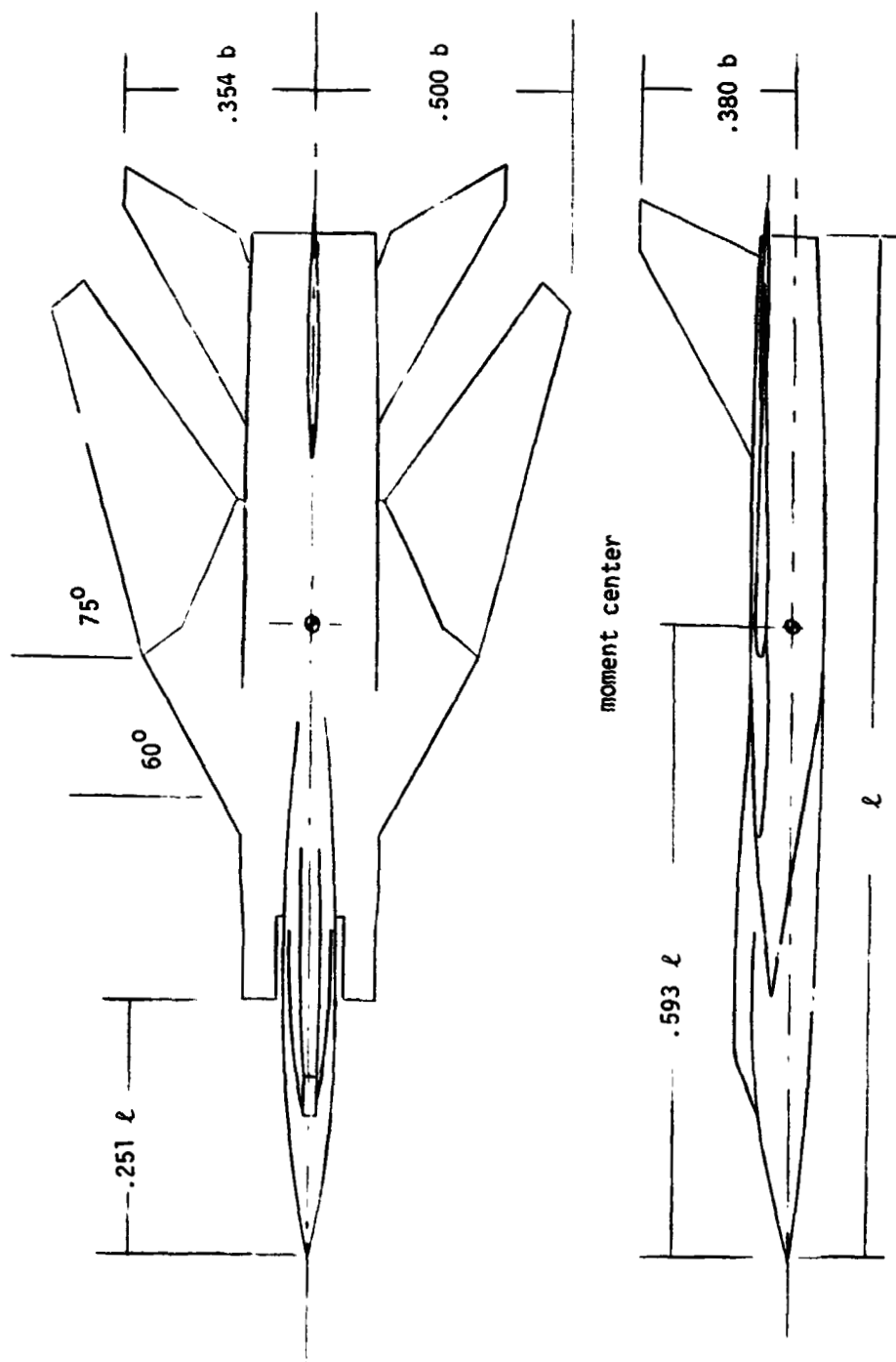
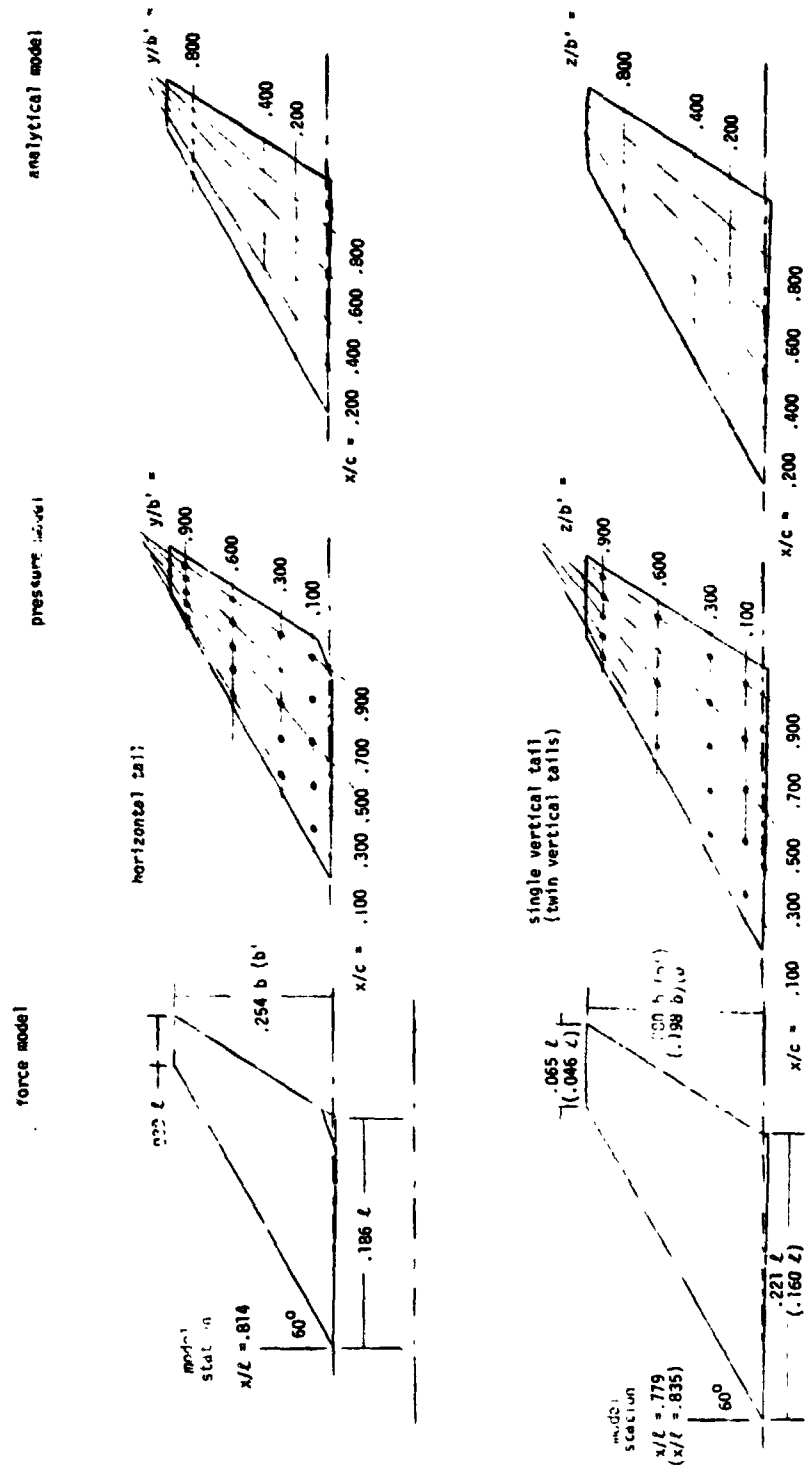


Figure 2. - Photographs of models installed in the Langley Unitary Plan wind tunnel.



(a) General configuration-single vertical tail

Figure 3.- Drawing of the model.



(b) Details of the tails

Figure 3.- Concluded.

Table 1  
AFT FUSELAGE ORIFICE LOCATIONS

Longitudinal station $x/l$	Top and bottom surfaces $y/b/2$				Left and right side surface $z/b/2$	
.820	-.196	-.098	0*	.098	.196	-.050    +.048**
.834						
.849						
.863						
.878						
.892						
.906						
.921						
.935						
.950						
.964						
.978						
.993						

\* No data recorded at any  $x/l$  for this position on top surface for configurations with single vertical tail

\*\* No data recorded at any  $x/l$  for this position on left surface for configurations with horizontal tail

Table 2  
TAIL SURFACE ORIFICE LOCATIONS

$x/c$	$y/b'$ or $z/b'$			
.100	.100	.300	.600	.900
.300	.100	.300	.600	.900
.500	.100	.300	.600	.900
.700	.100	.300	.600	.900
.900	.100	.300	.600	.900

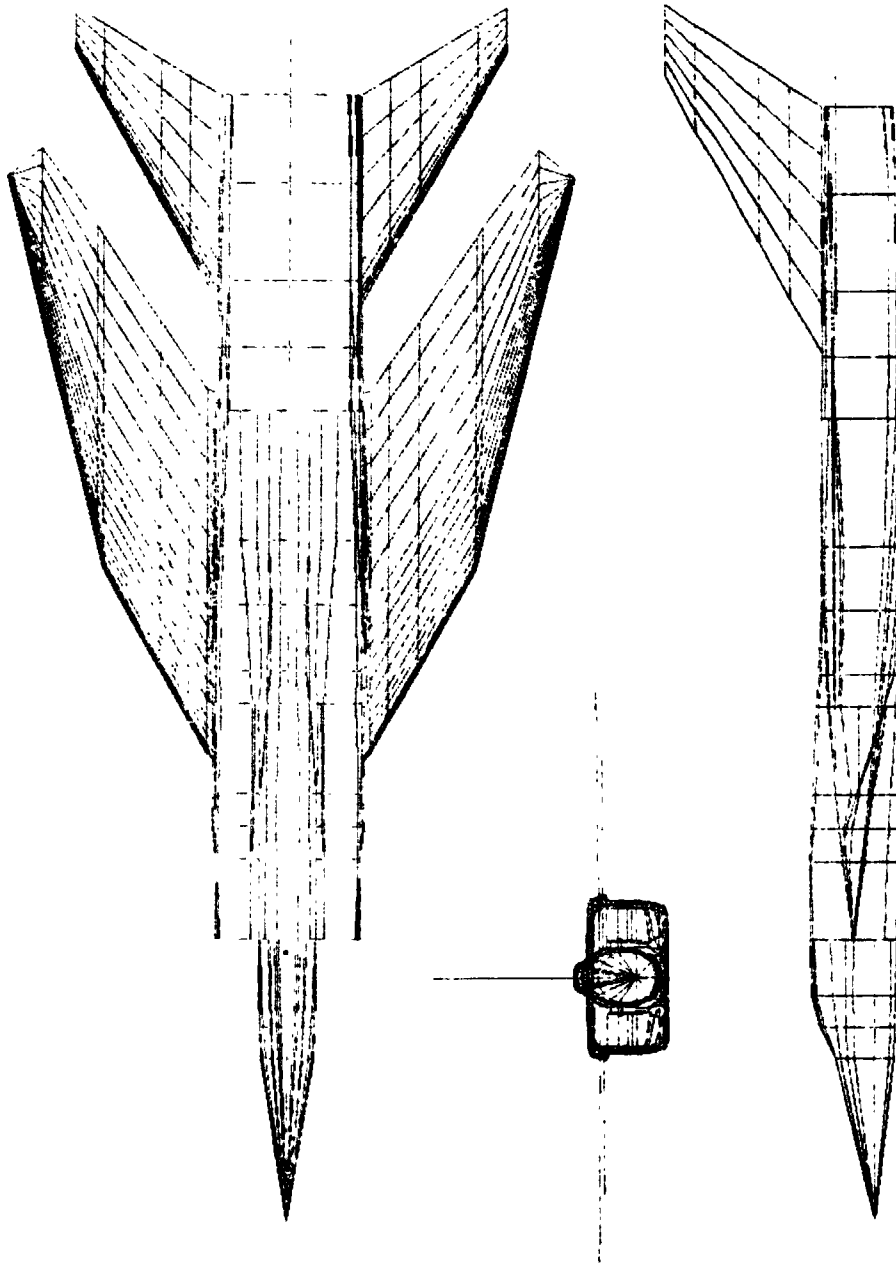


Figure 4. - Representation of the analytical model.



### Measurements and Instrumentation

Pressure model. - The diameters of the nickel-copper alloy tubing used to measure static pressures on the aft fuselage and tail surfaces were respectively .123 and .051 centimeters. The pressures were measured by means of differential pressure transducers with a  $\pm 2.5$  psi range. The transducers were referenced to a pressure near that of the test dynamic pressure which was measured by a mercury-filled manometer mounted outside the test section. In order to maximize accuracy, a differential pressure of about 2.5 psi was applied over the transducers and measured with the aid of another mercury-filled manometer also located outside the test section. The recorded test data fell within this differential pressure range. The accuracy of the test data was maintained within  $\pm 1.5$  psf.

Model angle-of-attack was measured by means of an accelerometer housed in the model nose chamber.

Force model. - Forces and moments on the model were measured by means of an internally mounted electrical strain gage balance which was rigidly attached to the tunnel sting-support system. Angle-of-attack was measured by using an accelerometer affixed to the sting-support system. Angles-of-attack were adjusted for sting-balance deflections due to aerodynamic loads.

General. - Angles-of-attack were adjusted for tunnel airflow misalignment.

### Data Acquisition

Force and pressure data. - The data presented herein tabulated from measured forces and pressures were acquired thru a computer operated data acquisition system, and represents the average of sixty frames of data recorded over a period of two seconds.

Flow visualization. - Visual data was recorded using the "vapor screen" technique. The vapor screen method (reference 5) focuses a thin vertical beam of concentrated lighting on the model which is immersed in airflow saturated with moisture. The light rays provide cutting planes through the "fog" that can then be visualized because the refracted light reflects the density changes in the flow. Flow disturbances such as shock fronts appear as discrete changes in lighting and vortices appear as darkened areas in the "vapor screen". The flow is photographed with cameras appropriately located inside or outside the test section. In addition, schlieren photographs of the tests were taken.

## CHAPTER III

### ANALYTICAL METHOD

#### General Background

Analytical methods in aircraft aerodynamics have been useful in the design cycle for a variety of aircraft configurations. But, these analytical configurations have been required to be relatively simple in shape. In references 6 thru 8 various methods are used to estimate the pressure distribution over simple aerodynamic shapes. The shapes considered are either bodies of revolution or lifting surfaces.

How to accurately predict the aerodynamic characteristics of bodies and lifting surfaces when placed in combination has been an area attracting considerable research. An example of such early efforts is reference 9 where a method for determining the lift characteristics on some wing-body-tail combinations is presented. The method of reference 9 is well substantiated by experimental results, but the applicable configuration shapes are limited to circular-cylindrical bodies of revolution with triangular, rectangular or trapezoidal wings. Although distribution of the airflow is not specifically treated, the authors placed considerable emphasis on the problem of determining the effect of wing vortices in the region of the tail. Recent efforts to better understand the behavior of vortices are reflected in references 10 and 11. A method for predicting vortex-lift is presented in reference 10, but has difficulty handling lifting surfaces with broken leading edge sweeps. Also, at supersonic speeds the method is quite sensitive to Mach number variations.

In reference 11, the author explores methods to determine the near-field wake structure resulting from the vorticity distribution immediately behind the lift-generating surfaces.

Some methods for predicting near-field pressures about bodies of revolution in supersonic flow are analyzed in reference 12. Whereas far-field prediction methods have been in general accord, prediction methods valid in the near-field have not. Several methods for determining near-field flow characteristics are based on the research efforts of G. B. Whitham (reference 13). Whitham uniquely combined supersonic linearized theory with a simplified characteristics theory to develop a method for calculating far-field pressures. Modifications which began the characteristics on the body surface instead of on the body axis extended Whitham's theory to the near-field and improved flow field predictions.

Whitham's method has been expanded by Woodward. Woodward's research efforts in references 14 thru 16 added singularity distributions to the lifting surface plane in an attempt to further improve the aerodynamic representation of the near-field. A Woodward analytical method was modified to simplify calculations and used in the supersonic transport studies in reference 17. In the method used for this investigation, reference 18, Woodward also attempts to include bodies of arbitrary shape. An evaluation of the subject Woodward method was made in reference 19 where the generally favorable conclusions were based on comparison of data obtained on wings, on bodies of revolution and on the pressure distribution on the wing of a wing-body-tail- configuration.

Predicting the flow over the tail, the focus of this investigation, is a more complex problem than that for the wing, primarily because of the difficulty in predicting aerodynamic interference on the tail.

Other analytical methods such as that discussed in reference 20 which was used to predict the pressure distribution about the B-1 airplane in supersonic flow may also provide accurate data estimates. The method of reference 20 is a finite difference method that solves a system of first-order hyperbolic partial differential equations in which a technique for predicting separated flow is included. To date, accurate results have been obtained on the test B-1 configuration using this method, but only about 80 percent of the body length has been analyzed. It should be mentioned that an extremely fine grid system was used in obtaining these results. The regions where the most complex flow exist, and the subject area of this investigation, has yet to be analyzed. For the three discrete conditions of attitude and Mach number predicted in reference 20, the partial calculations have used over 3 hours of computer computational time (CDC 7600 computer) and numerous man-hours have been required. The analysis of flow over the aft portions of the B-1 airplane is expected to be complete in early 1976. Only then can a thorough evaluation of the method be made.

The analytical method used in this investigation (reference 18) was selected because of its availability at Langley Research Center, because the computer program input is simple in that it is compatible with reference 21, and because previous use of the method with relatively simple geometries (reference 19) have provided acceptable results.

### The Woodward Method

The Woodward method used in this investigation is described in detail in reference 18. The approach taken, using potential flow theory, is to establish a system of linear equations which relates the magnitude of the velocity normal to the surface at each panel control point to the aerodynamic singularity strengths. The surface of the fuselage of the subject configuration is divided into a number of panels. On each fuselage panel, the strength of the potential function is assumed to be a constant source distribution and then the intervals can be evaluated over the element. The potential function strength must satisfy the boundary condition of tangential flow at the control point of each panel. The control point on the body(fuselage) is located at the centroid of each panel. Thus evolves a system of linear equations of unknown potential function strengths which are solved by an iterative procedure. Once the distribution of strengths is known, the velocities and then the pressure coefficients can be calculated at the control points.

The wing and tail surfaces are also divided into panels, but the potential function is a vortex distribution with linear variation in the streamwise direction. The numerical procedure for solutions to the vortex strengths is the same as for the fuselage. Although the option of singularity distributions on the surfaces of the lifting component is offered, it is currently available only for the subsonic case and is therefore not applicable for this investigation. In this investigation,

the wing and tail panels are located in the mean plane of the respective surfaces. Figure 4 illustrates the paneling scheme used for this investigation.

## CHAPTER IV

### RESULTS AND DISCUSSION

Because of the symmetry of the airflow and the symmetry of the model geometry under consideration in this investigation, the data presented herein will be only for the starboard side of the model.

#### Pressure Distributions

Afterbody fuselage.- The afterbody fuselage is relatively simple in design, resembles a distorted cylinder or square, and for research purposes is thought to be representative of current fighter aircraft. The distribution of pressure coefficients on the afterbody fuselage when void of tails is presented in figure 5. The data in figure 5 indicate that without tail interference, little flow variation with streamwise location ( $x/l$ ) exists at small angles of attack. At  $\alpha = 0^\circ$ , despite the interference of configuration forebody (nose, canopy, wedged inlets, centerbody) and wing, the pressure coefficients measured on the test model fuselage are comparable to the results in reference 22 for a body of revolution. This implies that at small incidence, forebody-wing interference effects about the body can be small or deteriorate rapidly with downstream position (in this Mach number region). Non-linearities in the pressure variation occur with increase in angle-of-attack, particularly at  $\alpha = 15^\circ$  on the fuselage top surface where comparatively large pressure gradients exist.



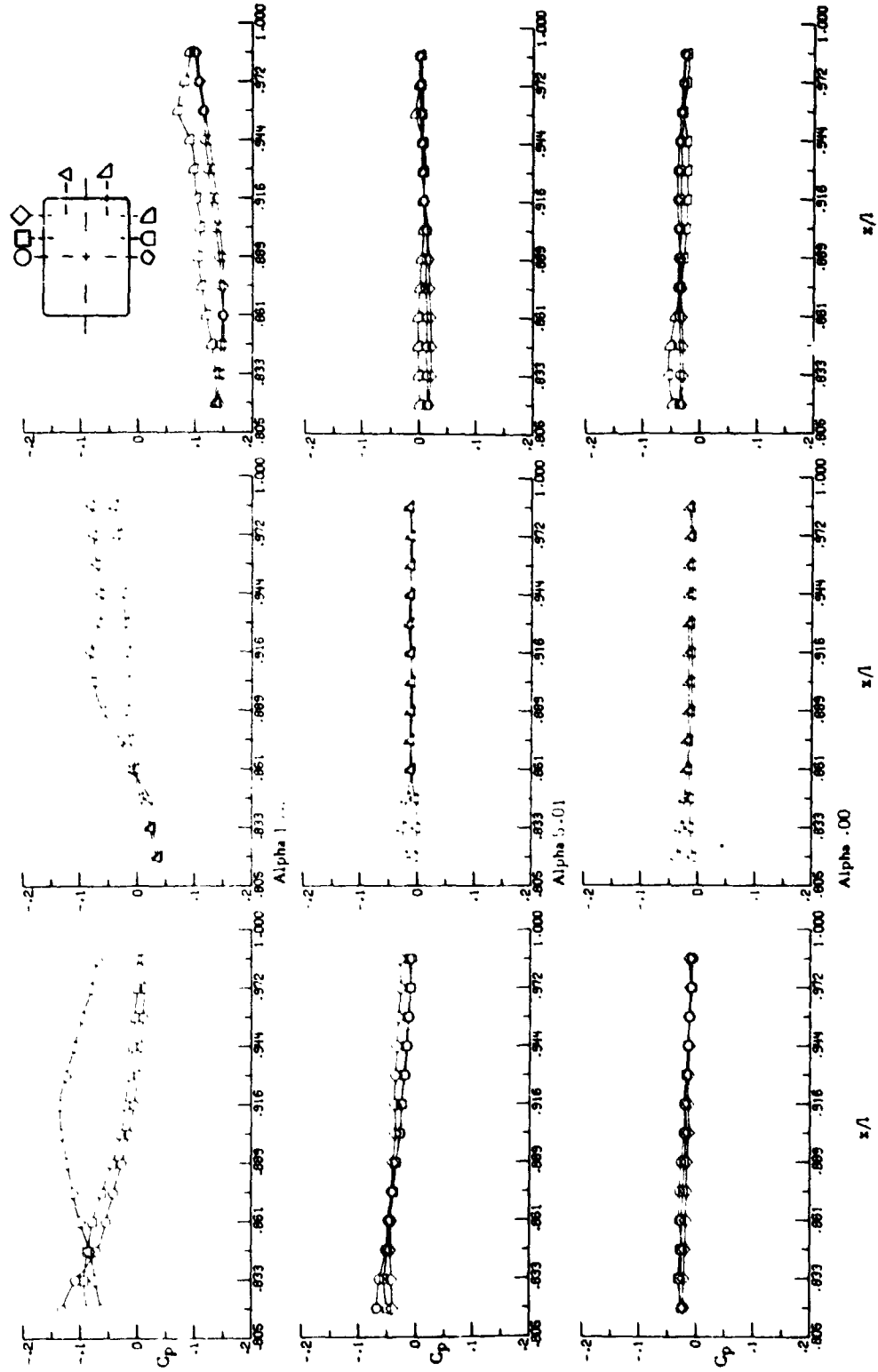
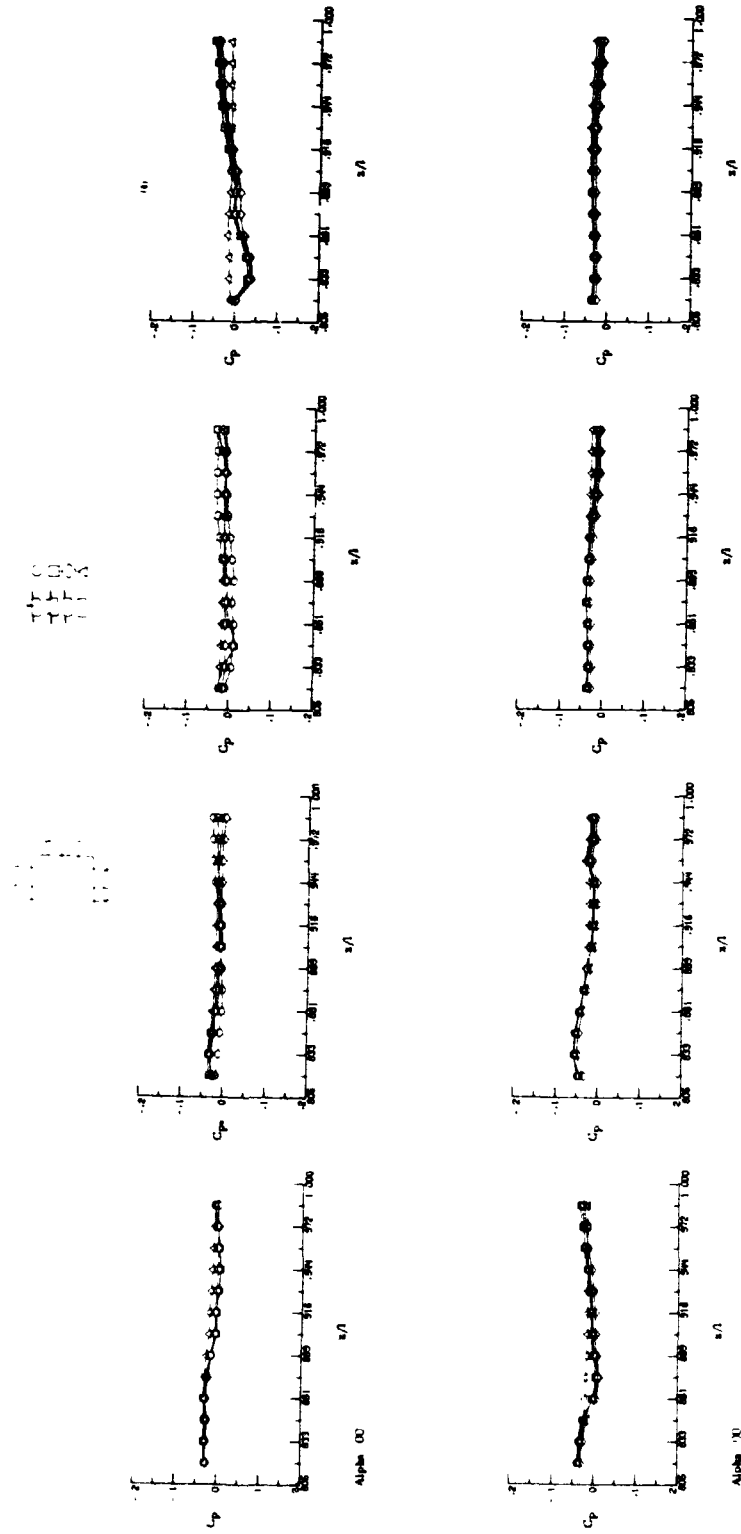


Figure 5.- Distribution of pressure coefficients on the afterbody fuselage without the presence of tails.

In figure 6, the effect of the various tail arrangements on flow about the afterbody is presented. The data show that the horizontal tail induces significant non-linearities in the pressure coefficients along the afterbody side. At  $\alpha = 0^\circ$ , where the horizontal tail effect appears minimal, maximum influence on the fuselage occurs in the region near the tail leading edge juncture with the fuselage. This higher pressure region on the fuselage is probably the result of this portion of the fuselage being behind the shock cone of the horizontal tail. The point along orifice row 4 and the point along orifice row 5 where the interference initially occurs define an angle which is a measure of the effective shock cone angle. The presence of a vertical tail in any test configuration is shown to significantly affect only flow on the fuselage top surface. The twin vertical tail arrangement, generally associated with the larger flow gradients, induces a region of expanded flow over the top surface and in particular near the tail-fuselage juncture(orifice row 2). The single vertical tail induces a higher pressure region on the fuselage near the airfoil leading edge( $x/l = .83$ ), but a lower pressure region near the airfoil trailing edge.

Vertical tail.- The position of the vertical tail relative to the forebody-wing wake can be crucial to aircraft stability. In reference 23 extensive wind tunnel force tests were performed on a similar combat fighter configuration to determine the aerodynamic effect of the vertical tail in various positions. The vertical tails used in reference 23 were similar to those used in this investigation. The starboard



(a)  $\alpha = 0$

Figure 6.- Comparison of pressure coefficient distributions on the afterbody fuselage with various tail arrangements.

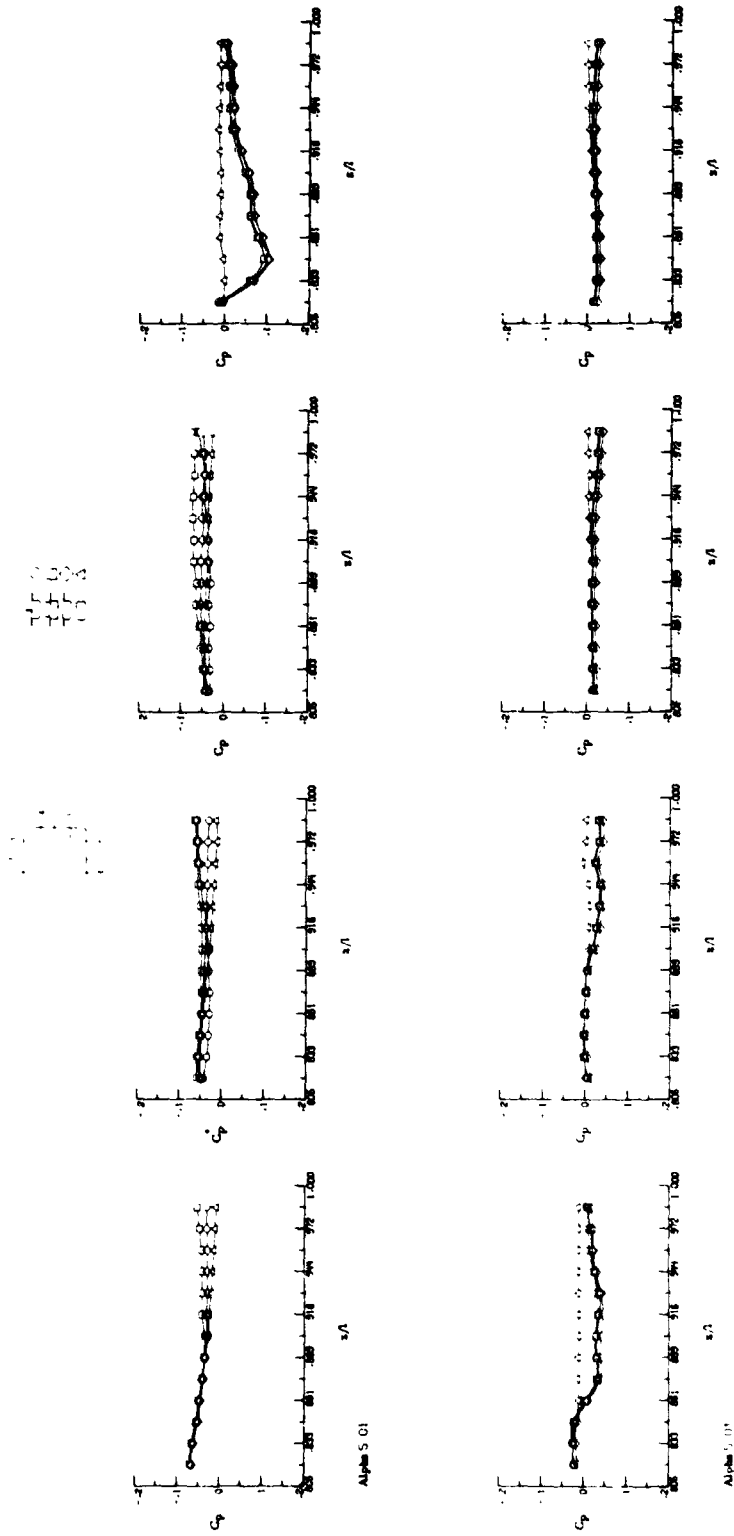


Figure 6.- Continued.

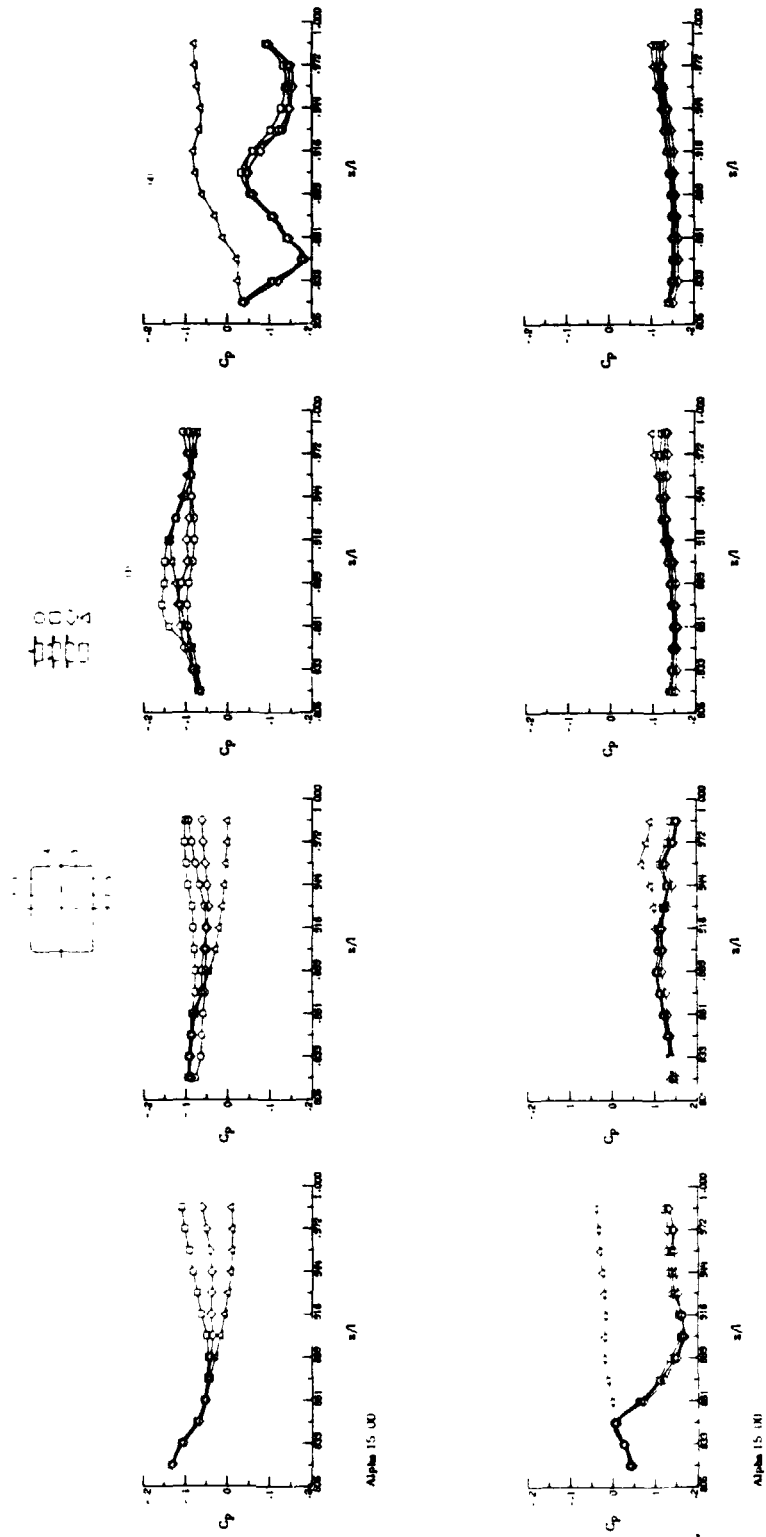
(c)  $\alpha = 15.0$ 

Figure 6.- Concluded.

surface flow conditions of the tails are indicated in figure 7 and the complete flow over the twin tail is indicated in figure 8.

Although the twin and single vertical tails are at different locations, the data of figure 7 show that at small angles of attack the pressure coefficients on the starboard surfaces are similar in value near the airfoil trailing edge. The twin tail exhibits higher pressures near the leading edge than the single vertical tail.

The differential pressure coefficients produced by the circulation of airflow about the twin vertical tail (figure 8) indicate an inboard directed side-force that increases with increase in angle-of-attack. Local flow regions near the fuselage show evidence of providing an outboard directed side-force near the airfoil trailing edge.

Horizontal tail. - Flow about the horizontal tail is shown in figure 9 for the configuration with the single vertical tail. The effect of the vertical tail positions on flow about the horizontal tail is depicted in figure 10 which shows that the single vertical tail effects the flow near the root chord leading edge and near the tip. The negative increment in  $C_p$  on both the upper and lower horizontal tail surfaces when in the presence of the single vertical tail is thought to be the result of shock interactions. The shock cone formed at the vertical tail leading edge propagates to intersect with other shocks, particularly those that emanate from the wing tip, to reduce local Mach number and decrease the local static pressures near the tip of the tail. Except as noted, the center vertical tail had essentially no effect on the horizontal tail

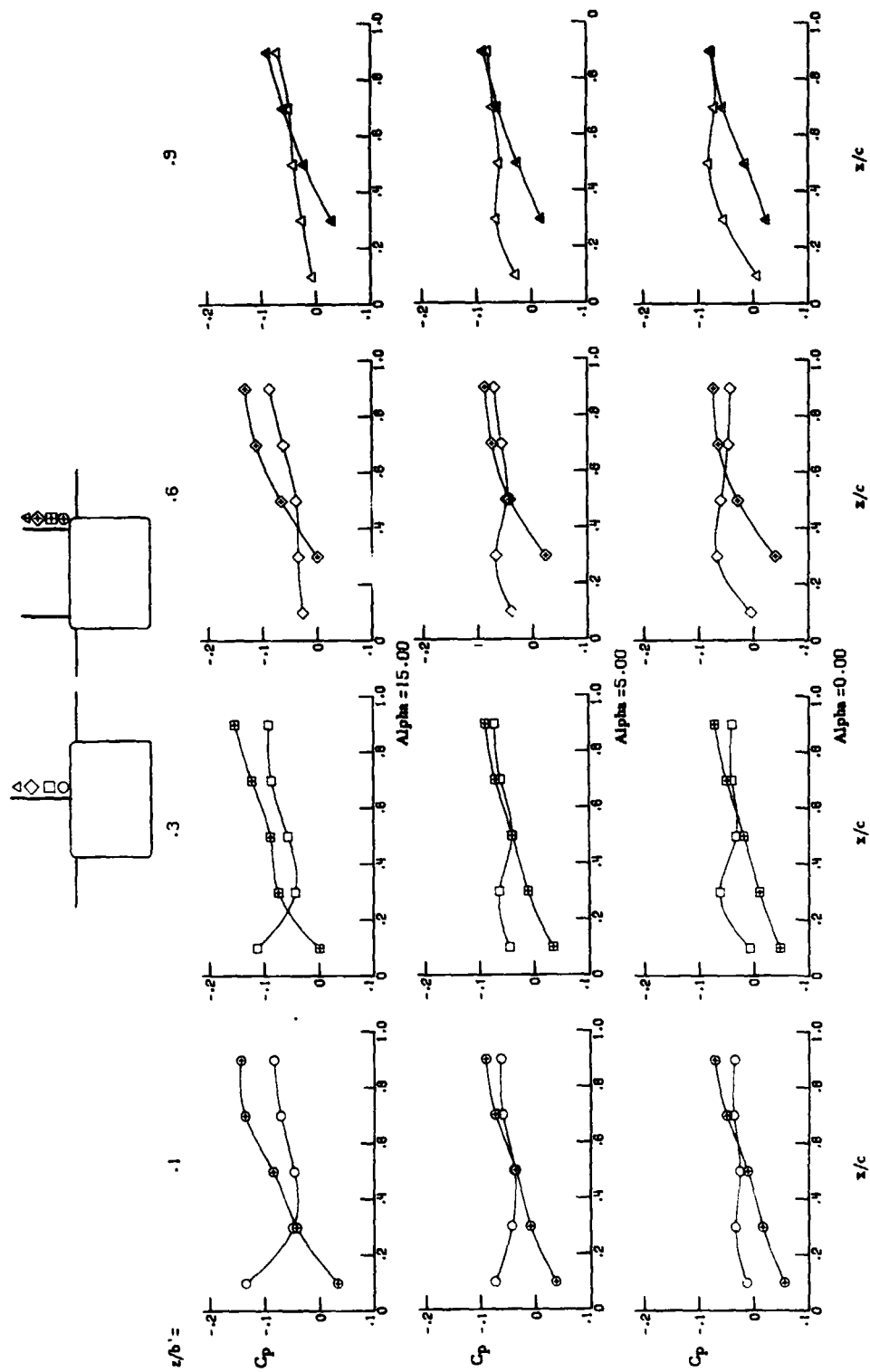


Figure 7.- Comparison of pressure coefficient distributions on the starboard surface of the various vertical tails.

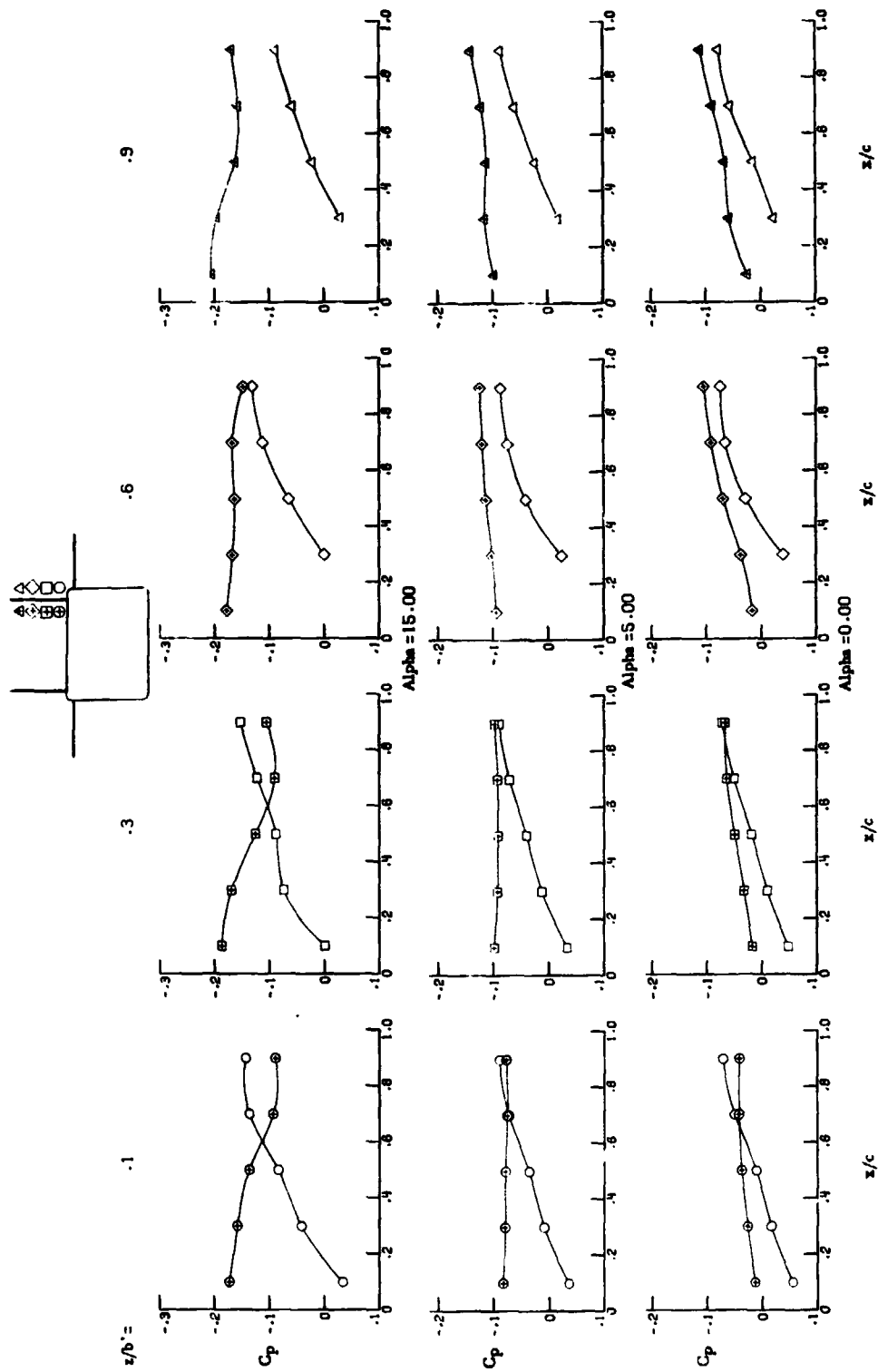


Figure 8.- Comparison of pressure coefficient distributions on the port and starboard surfaces of the twin vertical tail.



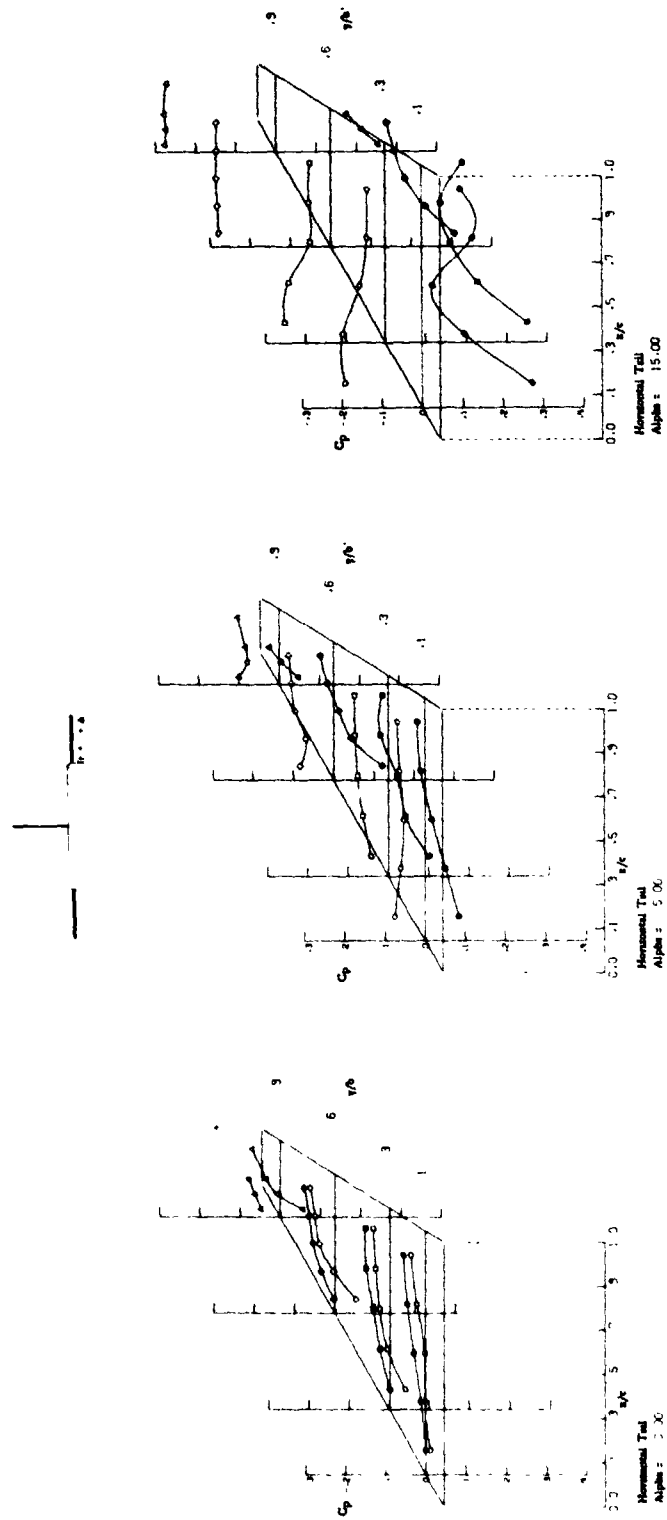
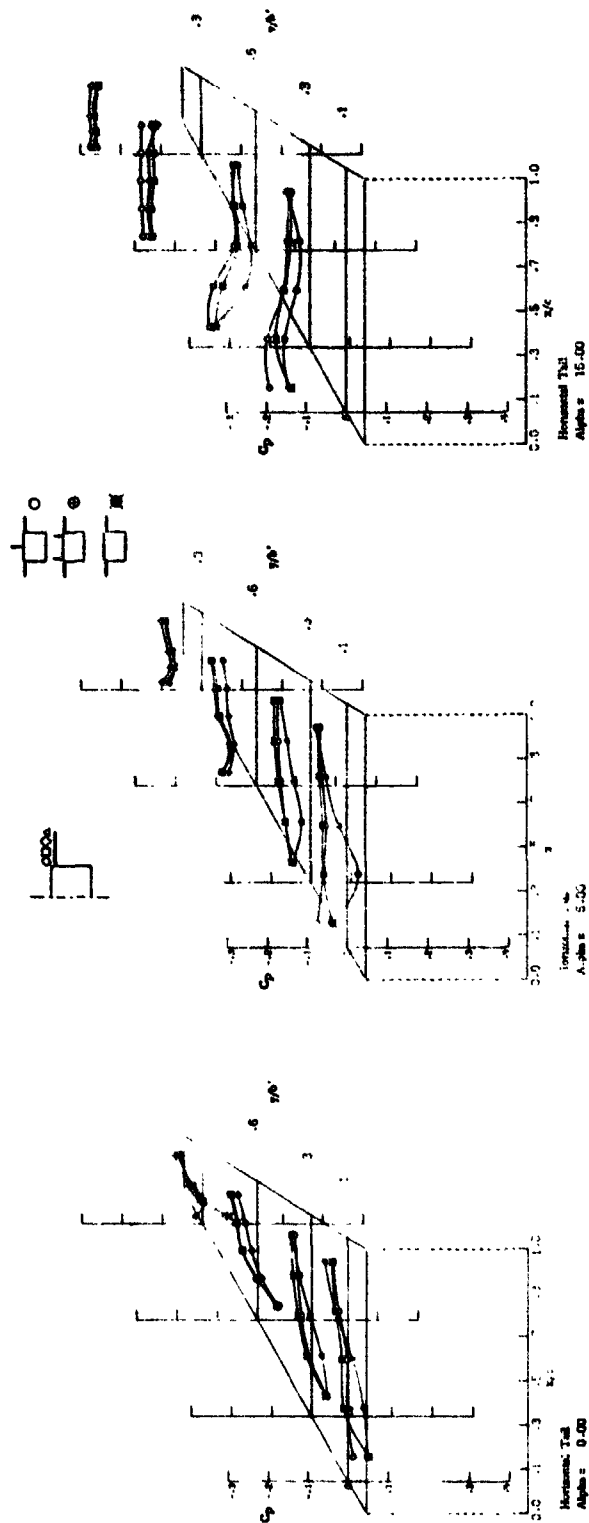
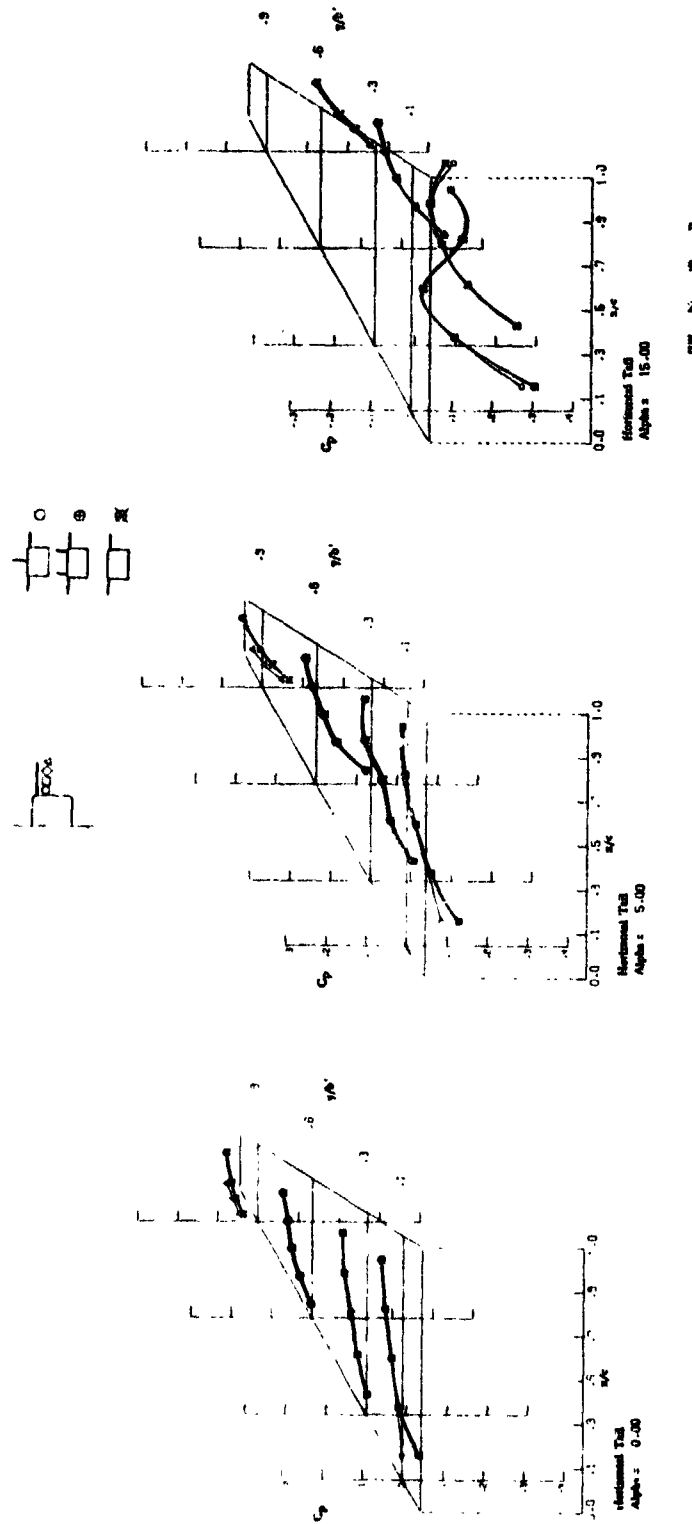


Figure 9.- Distribution of pressure coefficients on the upper and lower surfaces of the horizontal tail in the presence of the single vertical tail.



(a) upper surface

Figure 10.- Comparison of pressure coefficient distributions on the horizontal tail for various vertical tail arrangements.



(b) lower surface

Figure 10.- Concluded.

surface flow characteristics and the lower surface was unaffected for other tail variations (figure 10(b)). The twin vertical tail induces a higher pressure region over the horizontal tail upper surface that generally reaches a peak value near the 1/4 chord location. Regardless of the vertical tail arrangement (figure 10(a)), at  $\alpha = 15^\circ$  the tip portion of the horizontal tail upper surface appears to be in a region of detached flow as indicated by the lack of change in  $C_p$  with downstream travel ( $x/c$ ). The data in reference 24 for the comparable uncambered swept airfoil, which were recorded in the free stream, exhibit the basic flow trends as for the current tail in the wing-body wake.

### Flow Visualization

Vapor screen photographs. - The sequence of photographs in figure 11 were taken by a camera mounted inside the test section during "vapor screen" tests on the "force model". The photographs highlight flow at cutting planes perpendicular to the flow. The sequence of photographs taken at  $\alpha = 15^\circ$  were taken

(1) Immediately behind the wedged inlet tip

(2) Midway along the glove

and (3) Immediately behind the wing-glove juncture.

Although the reproduced photographs in this publication are not of particularly good quality (see Appendix A for enlarged photographs) careful examination of the above sequences will show the formation of vortex cores and vortex sheets depicted by the discrete dark areas at various positions along the model. Next in the sequence

(4) At the wing root trailing edge

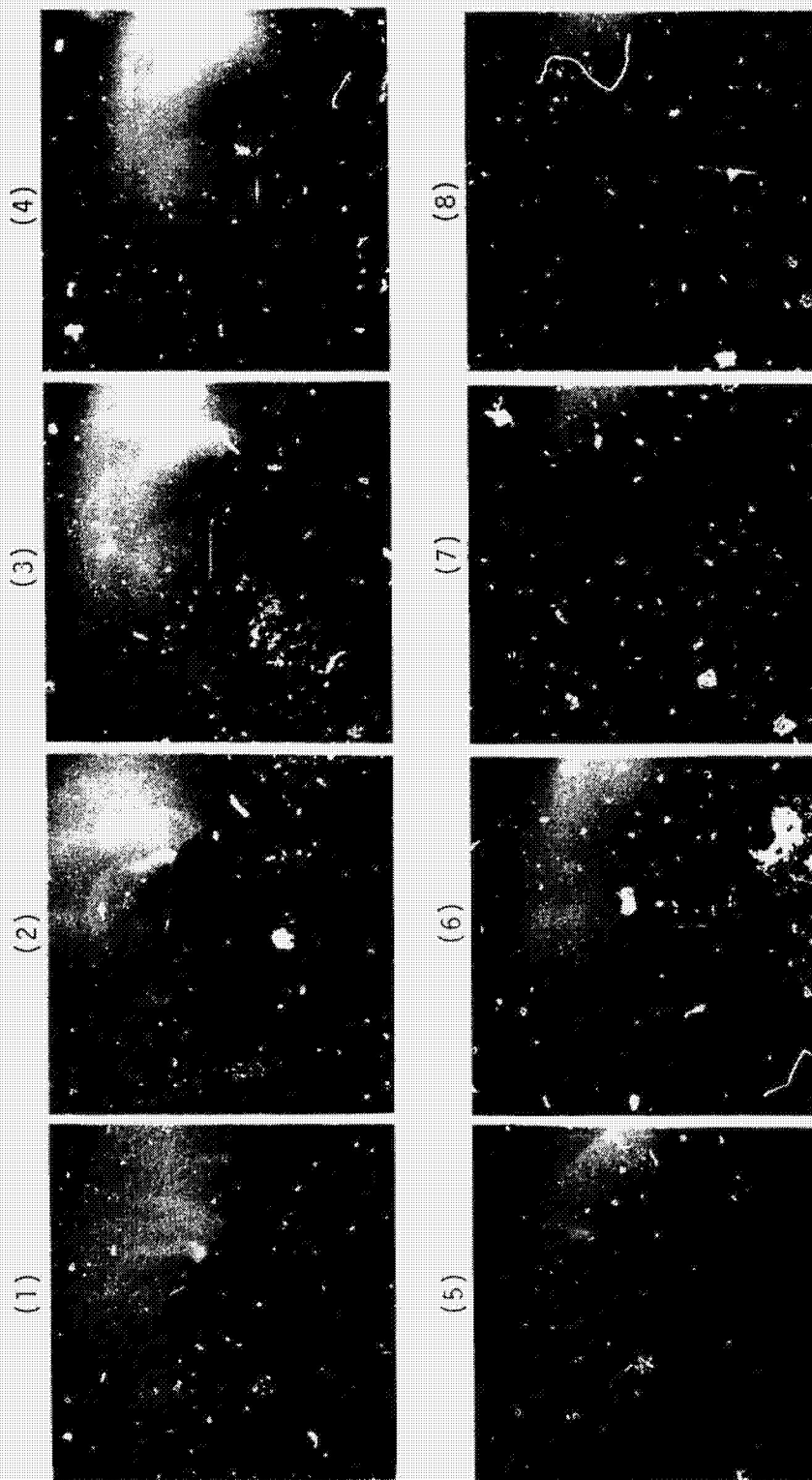


Figure 11.- Vapor screen photograph of the model at an angle-of-attack of 15 degrees.

can be seen an isolated vortex core between the fuselage and the wing trailing edge. This vortex is located below the model wing and is thought to form along the windward surface of the wedge-inlet ramp. Local circulation between the ramp and the fuselage apparently grows to sufficient strength to form a vortex core that travels a significant distance downstream.

The next three sequences

(5) Midway along the wing leading edge

(6) At the most spanwise tip of the wing

(7) At the most streamwise tip of the wing

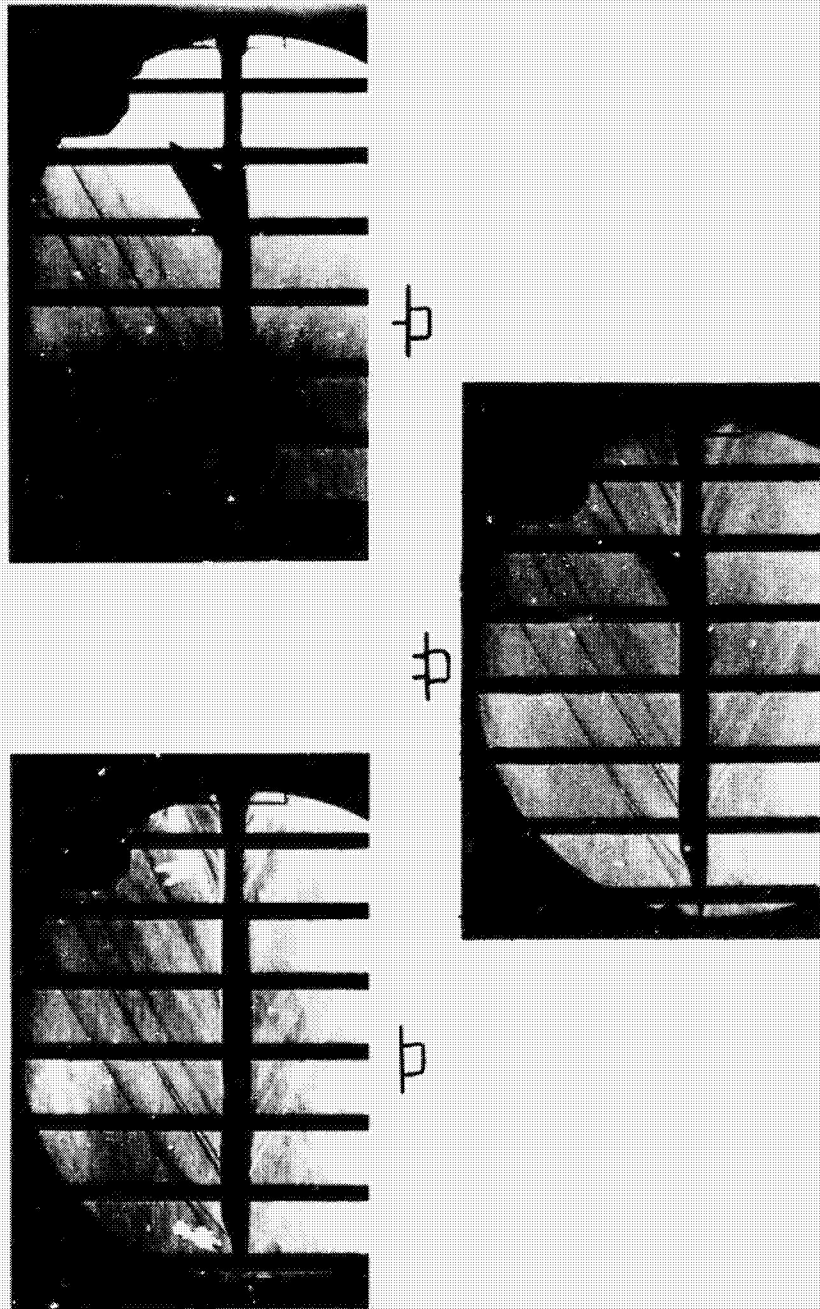
show strong vortices rolling over the wing leading edge that is classically described in reference 11. Sequences 6 and 7 also show apparently weaker vortices forming at the horizontal tail leading edge.

When also considering the sequence

(8) At the trailing edge of the vertical tail tip

it is quite apparent that a significant portion of the horizontal tail near the tip is immersed in its own vortex roll-up.

Schlieren photographs.- The schlieren photographs of figure 12(a) indicate by the light colored area extended over the fuselage top surface that at low angles of attack, regions of low energy air exist that persist in the presence of the vertical tail. In figure 12(b) further evidence of the aforementioned vortex core thought to form on the wedge-inlet ramp can be seen below the fuselage bottom surface (dark region that starts between the second and third vertical bars and travels downstream).



(a)  $\alpha = 0$

Figure 12.- Schlieren photographs of the model with various tail arrangements.





— (b)  $\alpha = 5.0$   
Figure 12.- Concluded.



## Force Tests

The force tests provide the integrated results of the model's aerodynamic characteristics. To determine the effect of the tails located on a given configuration, for example, the forces and the moments are obtained on the configuration with the tails on and tails off. Figure 13 shows the force test data where the effect of the horizontal and the single center-mounted vertical tails on the configuration can be seen.

A comparison of the configuration loading due to the tails obtained from the force tests with results obtained from the pressure tests is shown in Table 3. The simple analytical paneling scheme in figure 3(b) was used in this comparison. The change in loading on the afterbody fuselage due to the presence of the tails was also considered. Calculations were performed by using the equation

$$\Delta C_N = \frac{2 \sum \Delta C_p \times \text{local area}}{S}$$

The data is in excellent agreement although a rather sparse grid system was used in the numerical integration of the horizontal tail pressure data.

Table 3.

## COMPARISON OF FORCE AND PRESSURE TEST RESULTS ON NORMAL FORCE COEFFICIENT DUE TO HORIZONTAL AND SINGLE VERTICAL TAILS

$\alpha$ , deg	Pressure Data			Force Data
	horizontal $C_N$	tail body $\Delta C_N$	total $\Delta C_N$	$\Delta C_N$
0	-.005	-.001	-.006	-.005
5	.025	.002	.027	.026
15	.083	.004	.087	.090

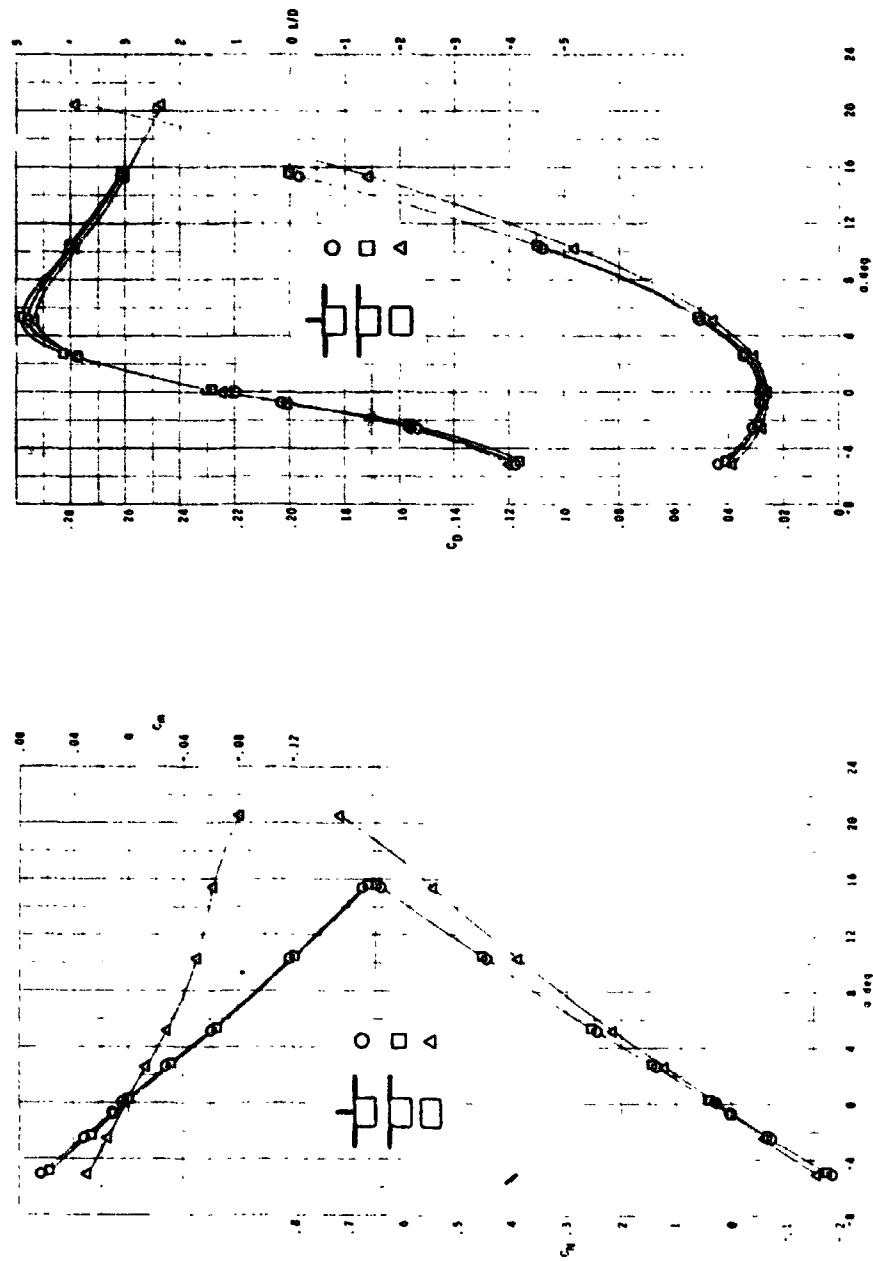


Figure 13.- Longitudinal aerodynamic characteristics of the model.

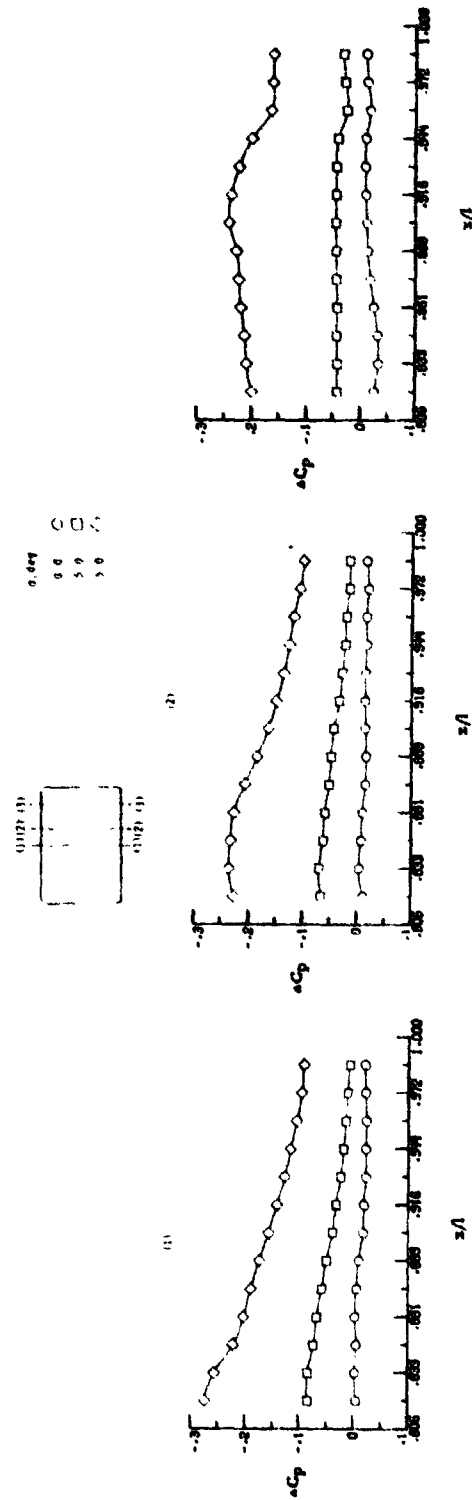
### Net Pressure Data

In figure 14 is presented the distribution of net pressure coefficients on the afterbody fuselage for various tail arrangements. The data indicate that the interference flow over the fuselage top surface due to the presence of the tails (previously discussed) generally results in an increase in positive normal force (negative  $\Delta C_p$ ) that is most prevalent near the model base. The twin vertical tails induce more incremental normal force than the single vertical tail.

Figure 15 shows that the twin vertical tail generally induces a positive increment in the normal force contribution of the horizontal tail. Net isobars on the horizontal tail in the presence of the single vertical tail are presented in figure 16. At  $\alpha = 0^\circ$  the peak loading appears to occur near the tip of the horizontal tail. With increase in angle-of-attack, the load concentration tends to move inboard and become more distributed over the tail surface. Peak chordwise values, as expected, occur at the leading edge.

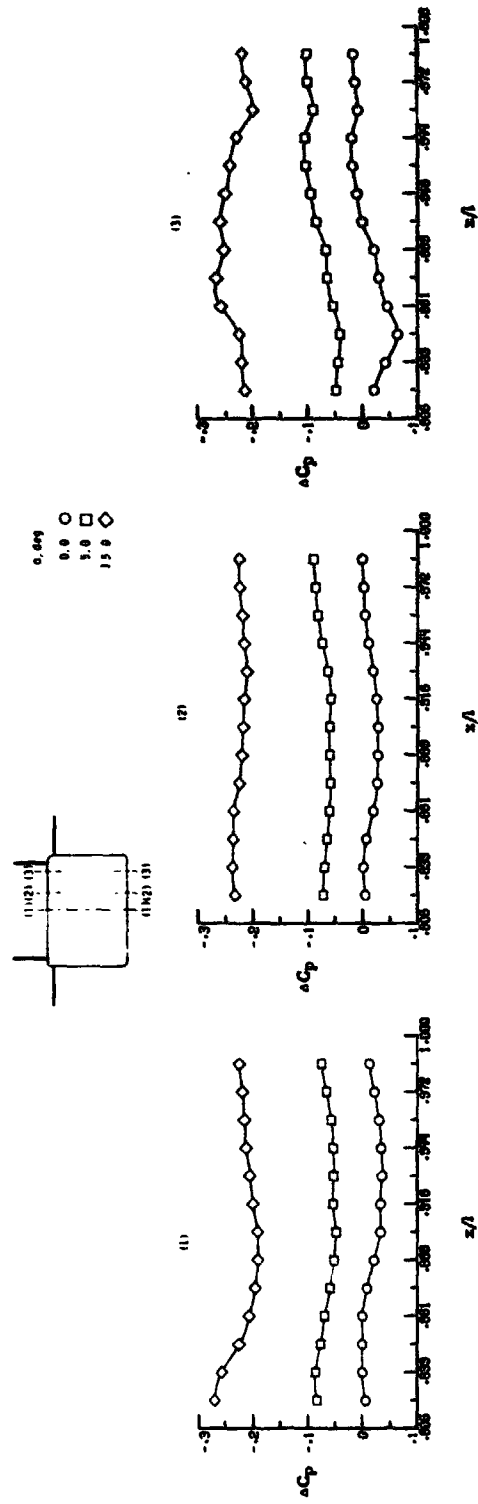
### Analytical Solution

Comparison with experimental data.— The analytical method as described in reference 18 was used to predict the flow about the model. In generating the numerical analysis model, emphasis was placed on obtaining predictions of pressure coefficients at positions that coincided with the orifice locations on the test model tail surfaces. Orifice matching was not attempted on the fuselage due to the added computer



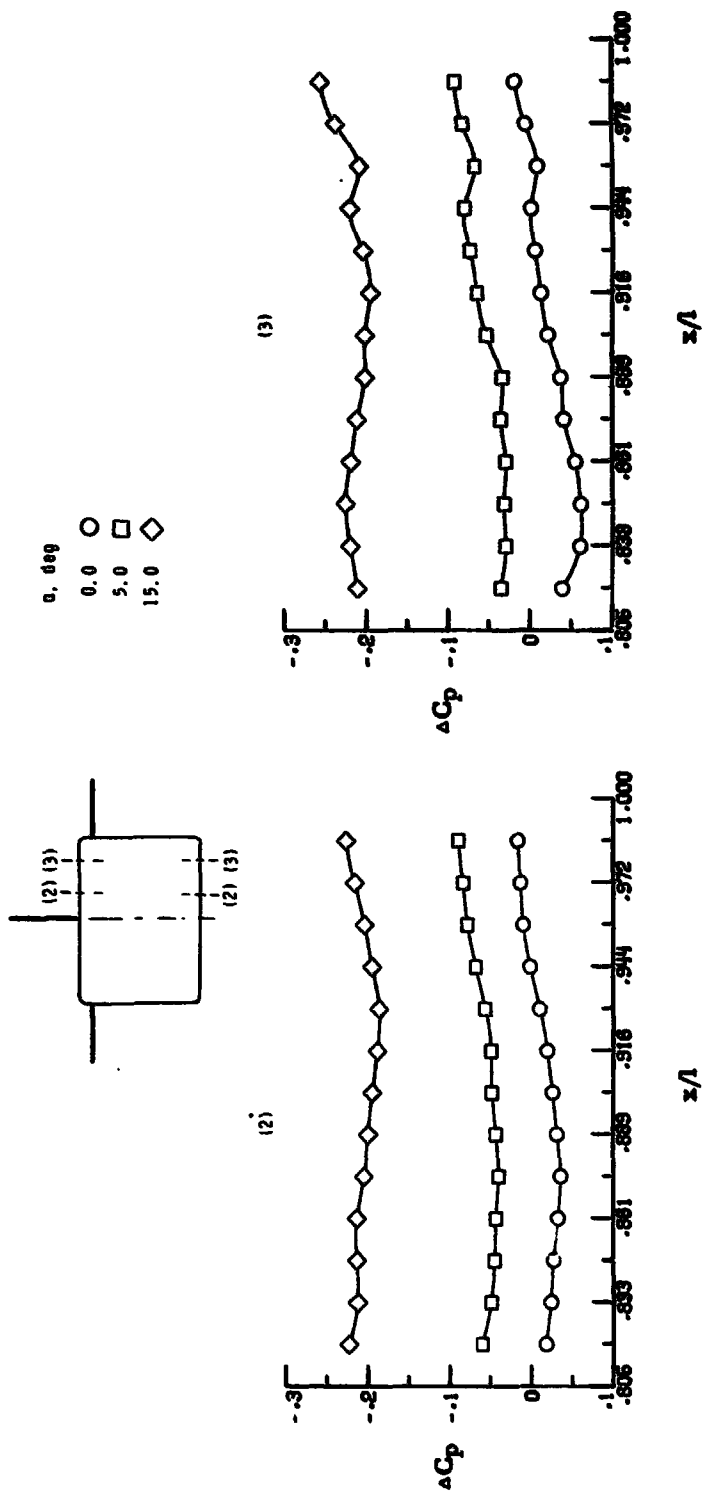
(a) no tails

Figure 14.- Distribution of net pressure coefficients on the afterbody fuselage with various tail arrangements.



(b) horizontal and twin vertical tails

Figure 14.- Continued.



(c) horizontal and single vertical tails

Figure 14.- Concluded.

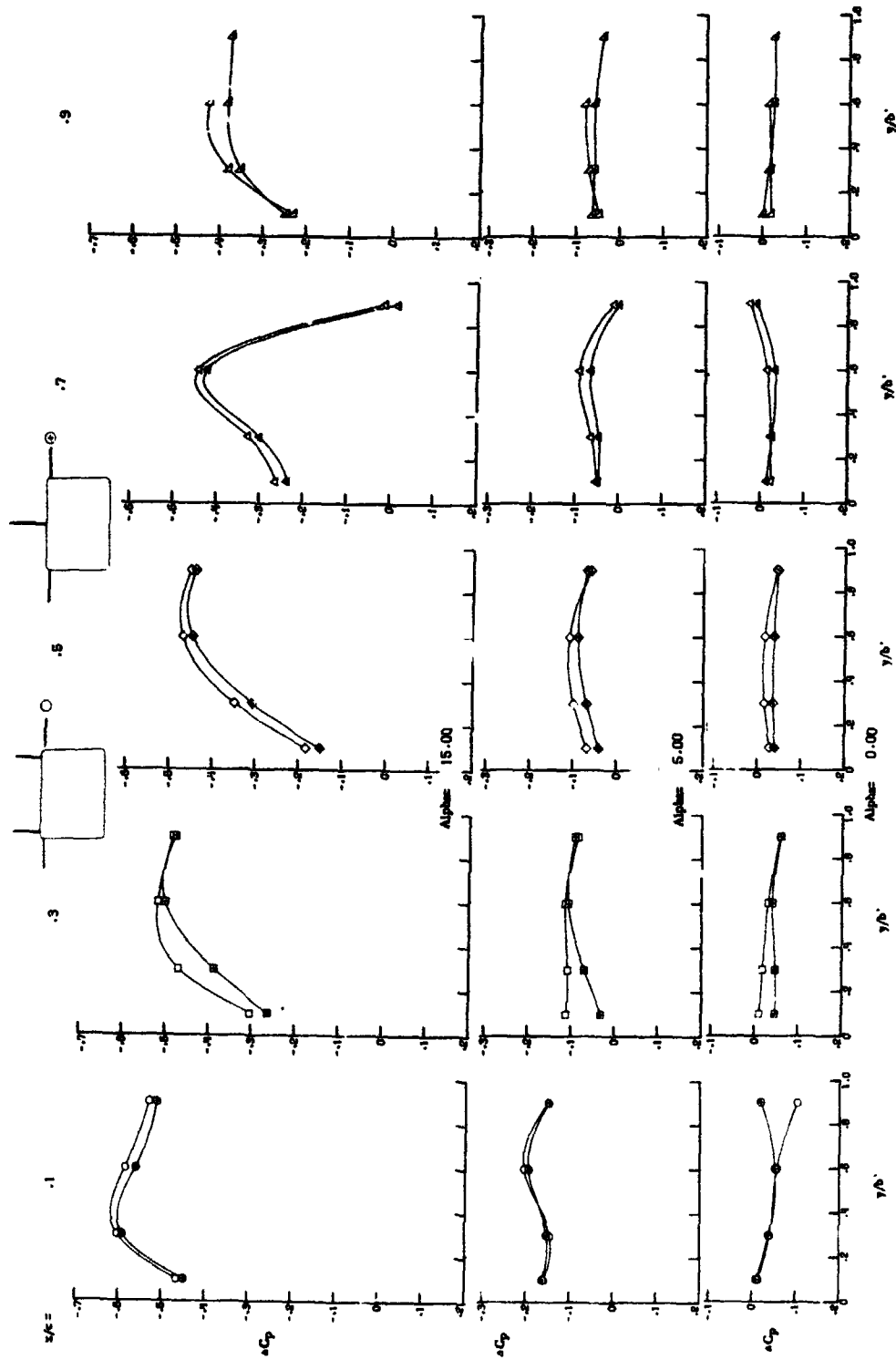


Figure 15.- Distribution of net pressure coefficients on the horizontal tail for various vertical tail arrangements.

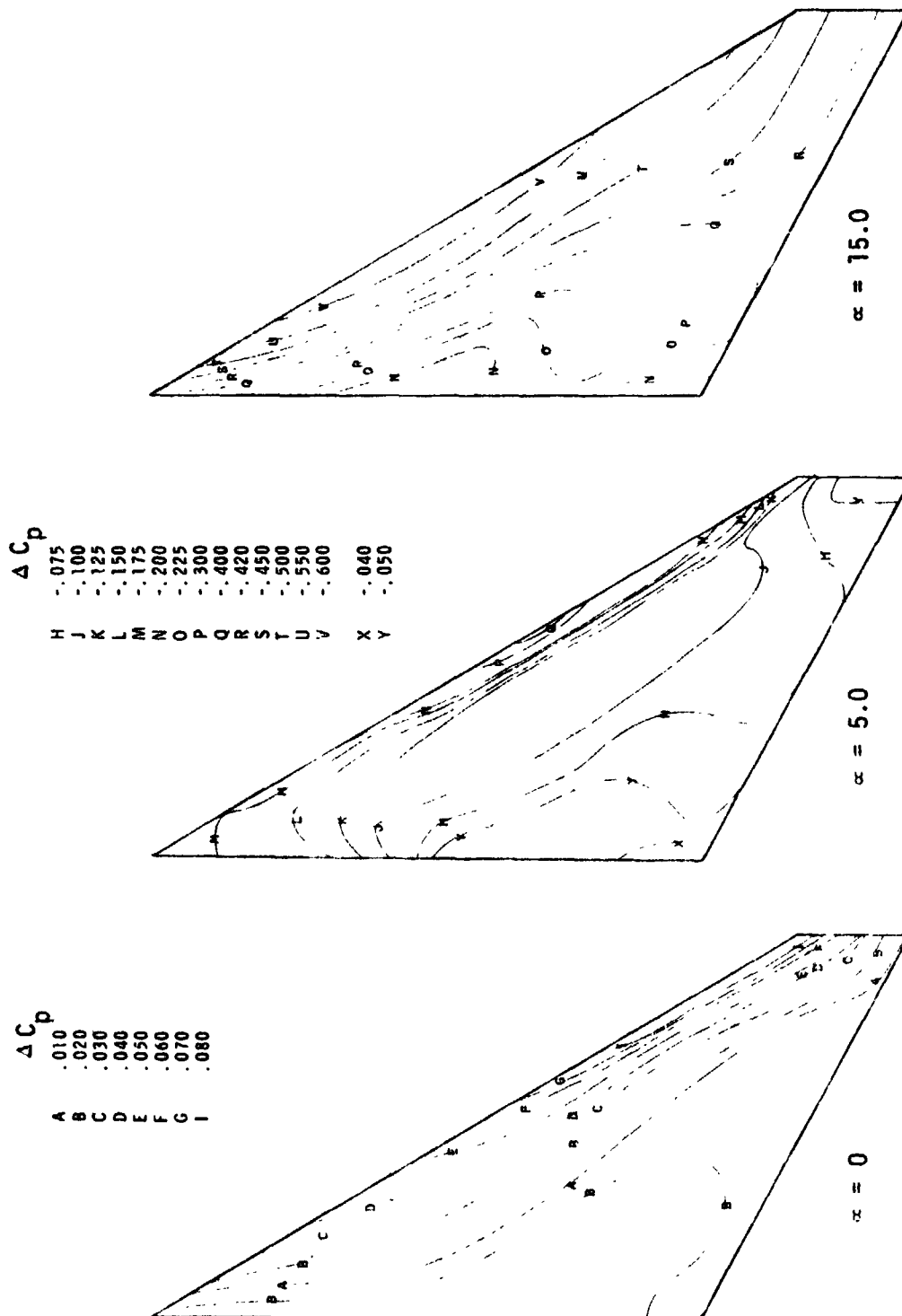


Figure 16.- Distribution of net isobars on the horizontal tail in the presence of the single vertical tail.



storage required and the significant increase in time required for calculations. It is felt that the analytical predictions for the afterbody fuselage are sufficiently representative of the flow that would be predicted if a more dense grid system were used. The analytical predictions for the body are representative of flow over the general surface areas whereas predictions over the tail surfaces are matched with experimental data for flow comparison at a point.

The predicted pressures over the afterbody fuselage (figure 17) generally well define the regions of the experimental data at small angles of attack. At  $\alpha = 15^\circ$ , the regions on the fuselage top surface continue to be well predicted, but the predictions for the fuselage side are scattered and do not provide adequate representation of the experimental data. Also at  $\alpha = 15^\circ$ , predictions of flow on the fuselage bottom surface generally tend to average higher pressures than indicated by experiment.

At small angles of attack and neglecting the region near the tip, pressures predicted over most of the horizontal tail are generally lower (more negative  $C_p$ ) than experimental values on the upper surface and larger than experimental values on the lower surface (figure 18). In the tip region, however, predicted values are generally much larger (more positive  $C_p$ ) than experimental values on the upper surface. At large angles of attack ( $\alpha = 15^\circ$ ) the predicted upper surface pressures are generally greater than those indicated by experiment.

The net result of the surface flows is shown in figure 19 where the predicted spanwise loading is greater (more negative  $\Delta C_p$ ) than experimentally determined loading at small incidence and less than experimental at large incidence ( $\alpha = 15^\circ$ ). The predicted data indicate an effective upwash (negative

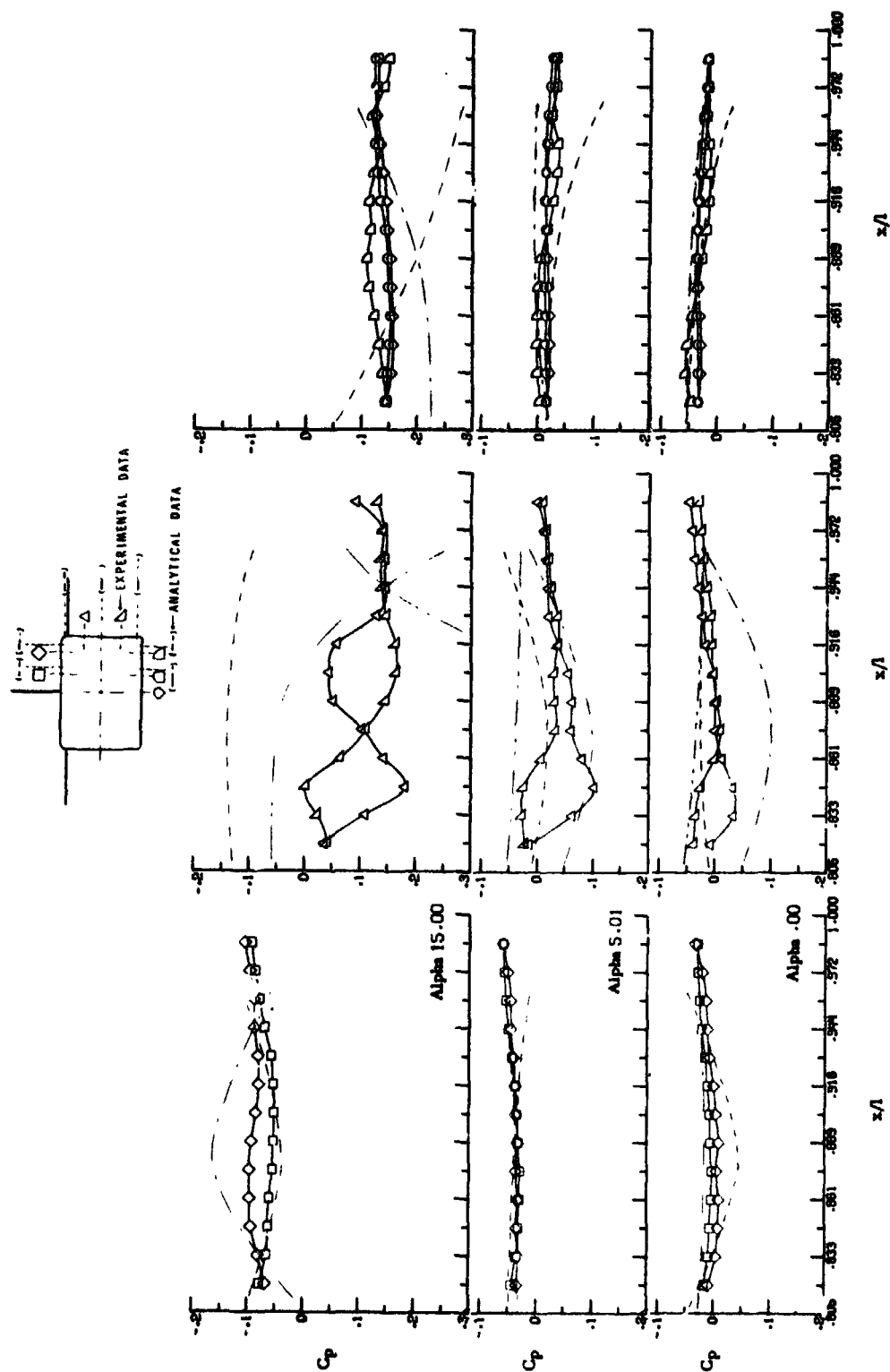


Figure 17.- Comparison of analytical predictions with experimental pressure data on the afterbody fuselage.

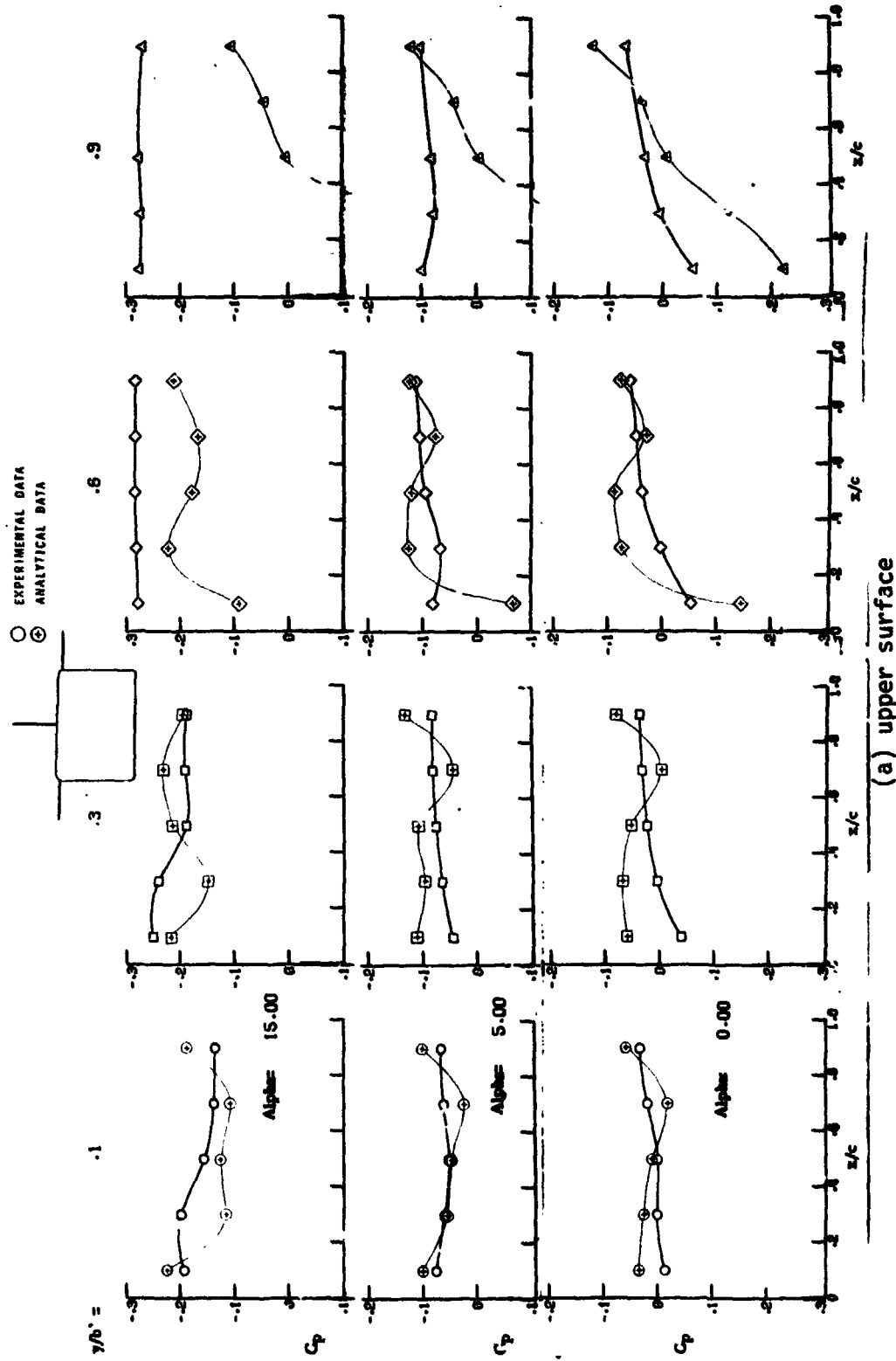
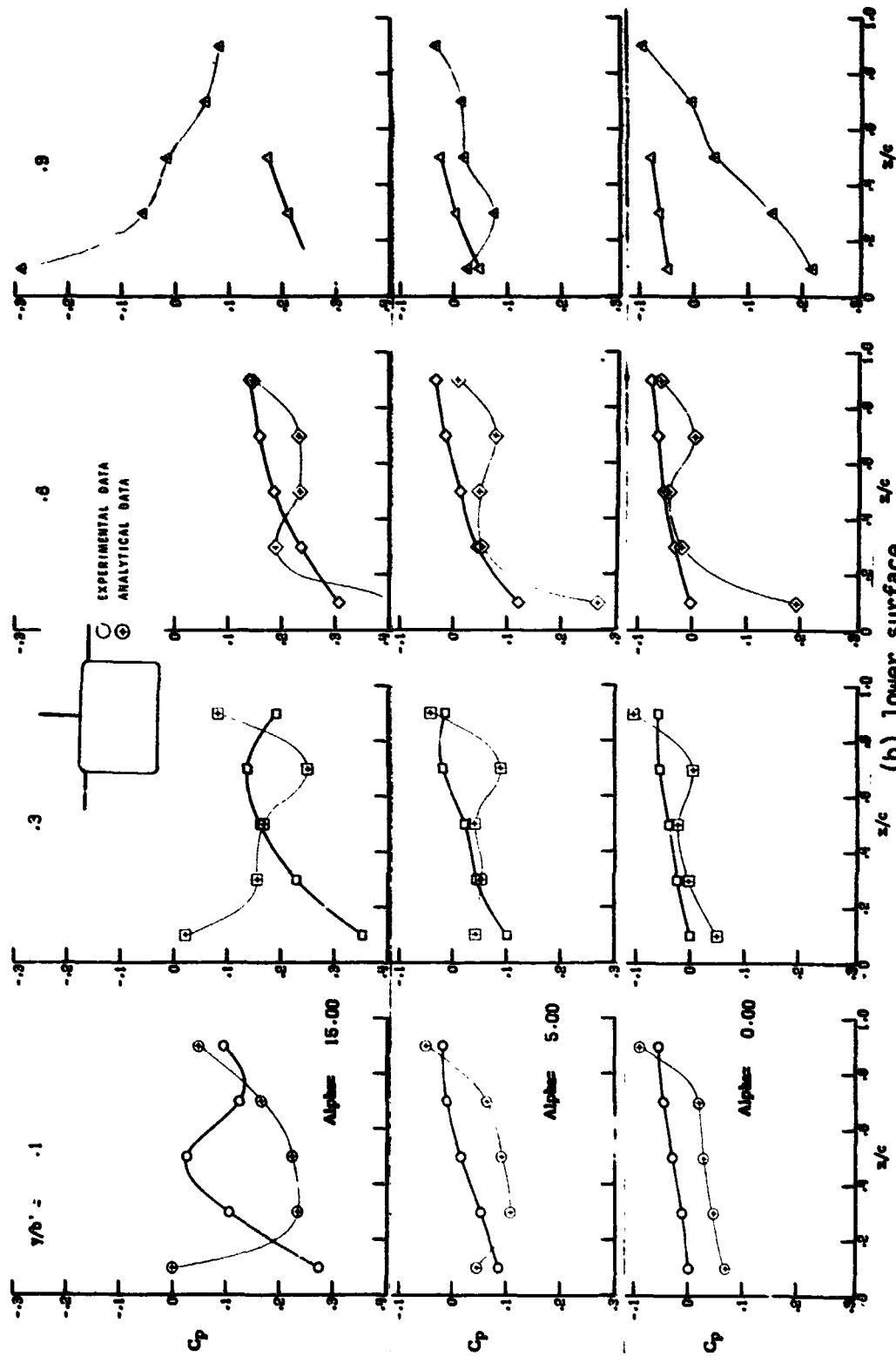


Figure 18.- Comparison of analytical predictions with experimental pressure data on the horizontal tail.



(b) lower surface  
 Figure 18.- Concluded.

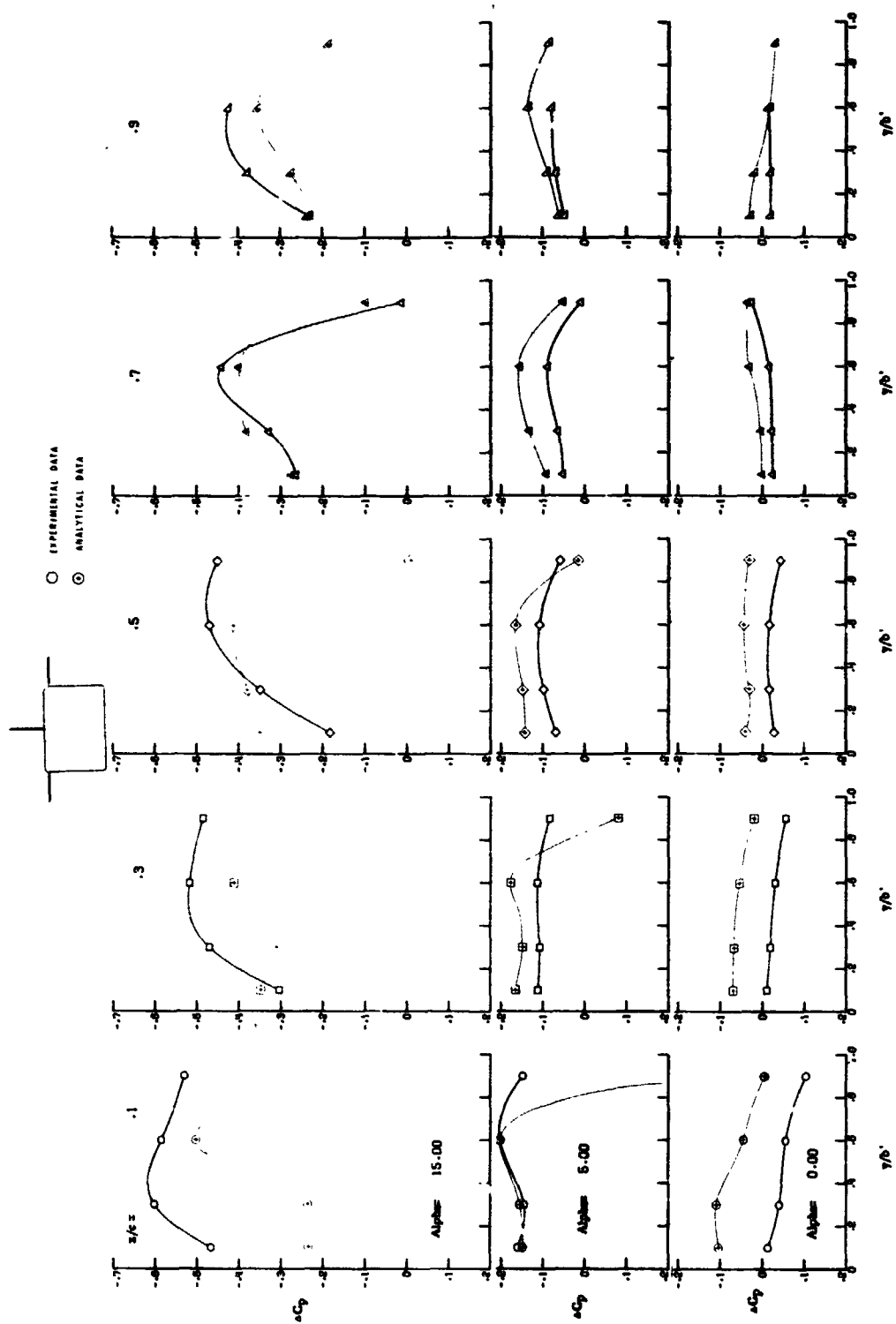


Figure 19.- Comparison of spanwise distribution of net pressure coefficients from experimental data on the horizontal tail with analytical predictions.

$\Delta C_p$  at  $\alpha = 0^\circ$ ) on the horizontal tail whereas experimental data clearly indicate downwash on the tail. This discrepancy can be accounted for in the analytical technique. The upstream influence on the various tail control points is determined by a system of Mach lines that define a region of aerodynamic influence. The resultant effect on the tail is attributed to the fact that in this method, apparently the upwash influence of the body is greater than the downwash influence of the wing.

Although the model has a complex analytical geometry, the predicted normal force and drag coefficients for the configuration presented in Table 4 compare well with experimental data (predicted data do not include vortex lift contribution). It should be noted, however, that a factor of two discrepancy in predicted  $C_m$  exists at  $\alpha = 5^\circ$  and  $15^\circ$ . Some factors which may account for this discrepancy are discussed in the next section.

Table 4  
COMPARISON OF SOME AERODYNAMIC RESULTS FROM FORCE  
TESTS WITH ANALYTICAL PREDICTIONS

$\alpha$ , deg	Coefficient	Force(Experimental)	Analytical
0	$C_N$	.027	.047
	$C_D$	.028	.026
	$C_m$	.005	.006
5	$C_N$	.245	.259
	$C_D$	.051	.052
	$C_m$	-.060	-.028
15	$C_N$	.640	.642
	$C_D$	.197	.205
	$C_m$	-.170	-.097

Analytical modeling and procedure. - The geometry of the configuration posed numerous handling problems for the analytical method. The gap between the model canopy and the port side of the wedge extension could not be analytically represented. The method currently cannot handle nacelles (or similar protuberances) and this gap was treated as though an extremely thin surface connected the canopy and the wedge. Thus the combined fuselage and the wedge inlet were analytically treated as comprising the fuselage. The broken sweep angle of the leading edge is such that for the test Mach number, the inboard portion of the wing has a subsonic leading edge and the outboard portion has a supersonic leading edge. Similar conditions exist for the wing trailing edge. Both geometric areas pose special and somewhat difficult procedures for the method.

The analytical model used for this investigation was relatively simple to construct to be compatible with reference 21. The computational data for the starboard half of the model is shown in Table 5.

TABLE 5  
ANALYTICAL MODEL COMPUTATIONAL DATA

No. of panels	Component
168	Fuselage
153	wing
36	horizontal tail
20	vertical tail

Computational time (CDC 6600 computer) to compute the data for the three model attitudes was approximately .44 hours.

The analytical method used provides an inviscid solution to the flow problem. Improvements in estimating the flow could be made by introducing viscous parameters into the procedure such as has been demonstrated in reference 20. Adjustments in the treatment of the aerodynamic influence coefficients on the fuselage and on the wing appear warranted to improve the prediction of downwash effects on the horizontal tail. The capability for better analytical representation of protuberances is also desirable.



## **CHAPTER V**

### **CONCLUDING REMARKS**

**An investigation of airflow over the aft portions of a variable sweep fighter aircraft configuration has been conducted at Mach number 2.16. Tests have been performed in the Langley Unitary Plan wind tunnel and an aerodynamic analytical prediction method used to provide information for correlation with the wind tunnel data. The results of this investigation indicate the following conclusions:**

- 1. At supersonic speeds, twin outboard located vertical tails should tend to provide more positive increments in normal force on the fuselage afterbody and the horizontal tail than a single center-line mounted vertical tail of similar planform shape.**
- 2. The use of the Woodward method currently in use at Langley Research Center for analysis of wing-body-tail configurations provides reasonable predictions of the pressure coefficients in a complex region of supersonic flow at small angles of attack. This computer program method is easy to use and requires relatively little computer time.**
- 3. Wind tunnel tests cannot at this time be adequately replaced by the analytical method used for understanding complex regions of supersonic flow. Flow visualization techniques**

are desirable aids in advancing the "state of the art" in analytical prediction methods. Desirable changes to increase the accuracy of the method include better analytical representation of geometric protuberances, revised treatment of aerodynamic influence coefficients on the body and on the wing, and the introduction of effective viscous parameters.

## REFERENCES

1. Braslow, Albert L.; and Knox, Eugene C.: Simplified Method for Determination of Critical Height of Distributed Roughness Particles for Boundary-Layer Transition at Mach Numbers From 0 to 5. NACA TN 4363, 1958.
2. Braslow, Albert L.; Hicks, Raymond M.; and Harris, Roy V., Jr.: Use of Grit-Type Boundary-Layer Transition Trips on Wind-Tunnel Models. NASA TN D-3579, 1966.
3. Ames Research Staff: Equations, Tables, and Charts for Compressible Flow. NACA Report 1135, 1953.
4. Anon: Technique for the Integral Casting of Pressure Instrumentation in Wind-Tunnel Models. NASA Brief 71-10247, 1971.
5. McGregor, I.: Flow Visualization in Wind Tunnels Using Indicators - Part IV. Development of the Vapour Screen Method of Flow Visualization in a 3 ft. x 3 ft. Supersonic Tunnel, AGARDograph 70, April 1962.
6. Peterson, Robert L.: Pressure Distribution on Warped Wings at Supersonic Velocities, MIT Nav. Sup. Lab. Tech. Rpt. 389, 1960.
7. Van Dyke, Milton D.: First- and Second-Order Theory of Supersonic Flow Past Bodies of Revolution, Journal of the Aeronautical Science, Vol. 18, No. 3, 1951, pp. 161-178.
8. Lighthill, M.J.: Supersonic Flow Past Bodies of Revolution, R. & M. No. 2003, British A.R.C. 1945.
9. Pitts, William C.; Nielsen, Jack N.; and Kaattari, George E.: Lift and Center of Pressure of Wing-Body-Tail Combinations at Subsonic, Transonic, and Supersonic Speeds. NACA Report 1307, 1957.
10. Polhamus, Edward C.: Predictions of Vortex-Lift Characteristics Based on a Leading Edge Suction Analogy. AIAA Paper No. 69-1133, October 1963.
11. Rossow, Vernon L.: Aerodynamic Analysis Requiring Advanced Computers - Part II. Survey of Computational Methods for Lift-Generated Wakes. NASA SP-347, March 1975, pp. 897-924.
12. Mack, Robert J.: A Study of Methods Which Predict Supersonic Flow Fields From Body Geometry, Distance, and Mach Number. NASA TN D-7387, November 1973.

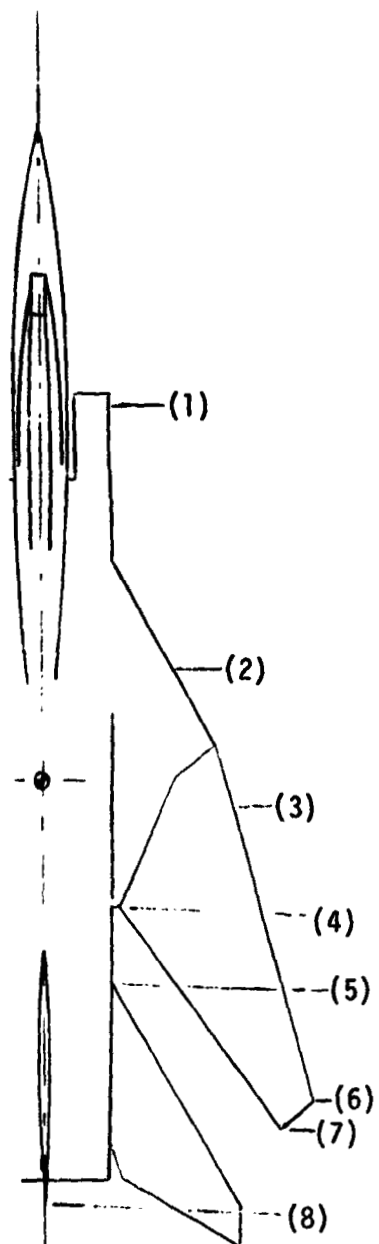
13. Whitham, G.B.: The Flow Pattern of a Supersonic Projectile. Commun. Pure. Appl. Math., Vol. V. No. 3, August 1952, pp. 301-348.
14. Woodward, F. A.; and Larson, J. W.: A Method of Optimizing Camber Surfaces For Wing-Body Combinations at Supersonic Speeds. Part I-Theory and Application. Doc. D6-10741, Pt. I, Boeing Co., 1965.
15. Carmichael, R. L.; and Woodward, F. A.: An integrated Approach to the Analysis and Design of Wings and Wing-Body Combinations in Supersonic Flow. NASA TN D-3685, October 1966.
16. Woodward, F. A.; Tinoco, E. N.; and Larson, J. W.: Analysis and Design of Supersonic Wing-Body Combinations, Including Flow Properties in the Near Field. Part I - Theory and Application. NASA CR-73106, August 1967.
17. Manro, Marjorie E.; Moulijn, Johan P.; and Knittel, James D.: SST Technology Follow-On Program - Phase I. Vol. 2 - Pressure Distributions on a Delta Wing-Horizontal Stabilizer Combination at Mach Numbers From 0.3 to 2.9. FAA-SS-72-30-02, July 1972.
18. Woodward, F. A.: An Improved Method for the Aerodynamic Analysis of Wing-Body-Tail Configurations in Subsonic and Supersonic Flow. Part I - Theory and Application. NASA CR-2228, May 1973.
19. Breedlove, William J., Jr.: A Report of Five Summer Research Projects. An Evaluation of Woodward's Improved Method for the Aerodynamic Analysis of Wing-Body-Tail Configurations in Subsonic and Supersonic Flow. Old Dom. U. Tech. Rpt. 73-M1, Nov 1973, pp. A1-A88.
20. D'Attore, L.; Bilyk, M.A.; and Sergeant, R.J.: Three Dimensional Supersonic Flow Field Analysis of the B-1 Airplane by a Finite Difference Technique and Comparison With Experimental Data. AIAA Paper No. 74-189, January 1974.
21. Craidon, Charlott B.: Description of Digital Computer Program For Airplane Configuration Plots. NASA TM X-2074, September 1970.
22. Harris Roy V., Jr.; and Landrum, Emma Jean: Drag Characteristics of a Series of Low-Drag Bodies of Revolution at Mach Numbers From 0.6 to 4.0. NASA TN D-3163, December 1965.
23. Feryn, Maurice O.; and Fournier, Roger H.: Aerodynamic Characteristics at Mach Numbers From 2.50 to 4.63 of a Fighter Configuration With Various Vertical- and Horizontal-Tail Arrangements. NASA TM X-1378, May 1967.
24. Carlson, Harry W.: Pressure Distributions at Mach Number 2.05 on a Series of Highly Swept Arrow Wings Employing Various Degrees of Twist and Camber. NASA TN D-1264, May 1962.

## **APPENDIX A**

### **VAPOR SCREEN PHOTOGRAPHS**

**This appendix provides an enlargement of the visual data presented in the text as Figure 11 and discussed on pages 31 thru 33. The data were recorded at an angle of attack of 15 degrees because the flow could more readily be seen and recognized than at lower angles of attack. The sequence of photographs presented depicts the flow at the various positions along the model in accordance with the numbered stations on the model sketch.**

**The shock fronts appear as discrete changes in lighting in the photographs, whereas the vortices appear as dark areas. (Familiarity with the model geometry is suggested before analysis of the photographs is attempted. Model shadows and the black-painted model itself may also appear as dark areas.)**

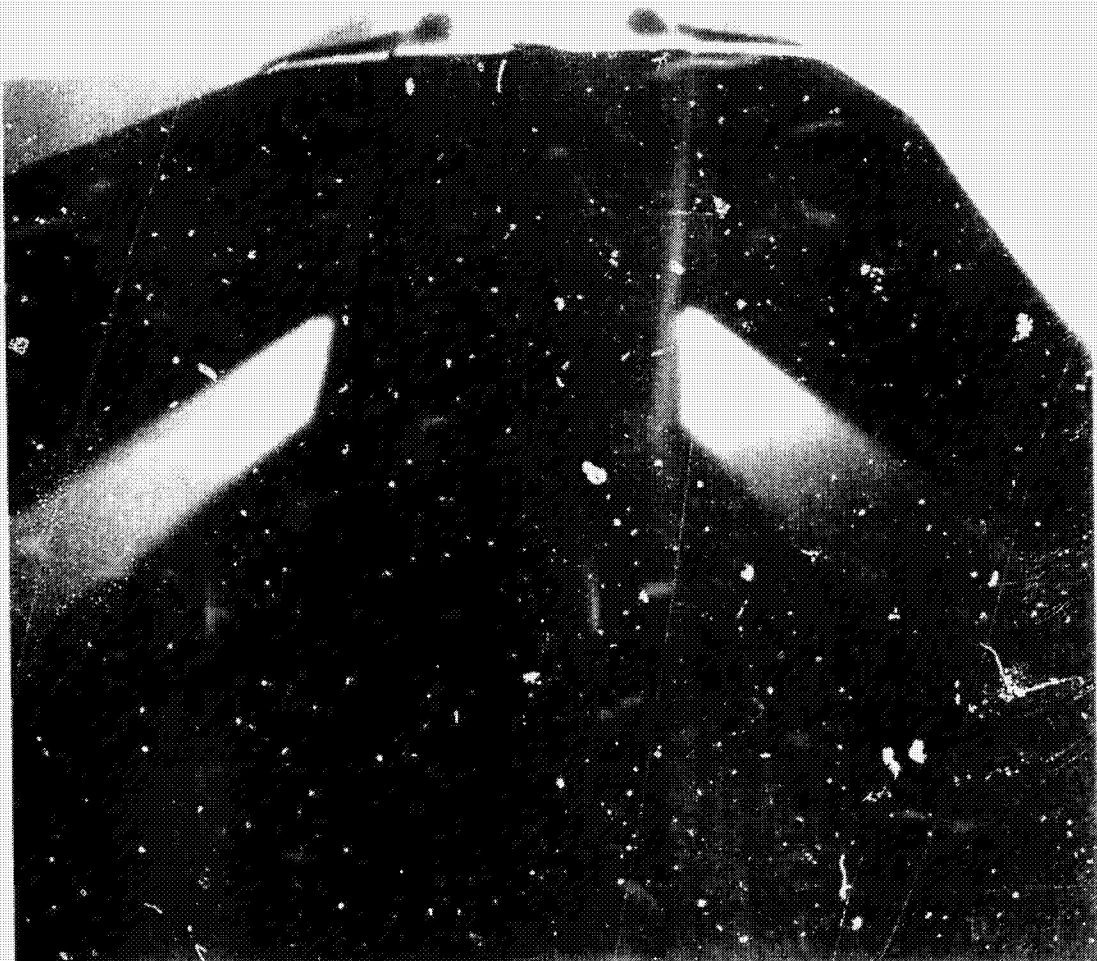


Half-model sketch.

(1)



(2)





60

REPRODUCIBILITY OF THE  
ORIGINAL IS POOR

(3)



61

PROPERTY OF THE  
U.S. POOR

(4)



62

REPLICA  
ORIGINAL

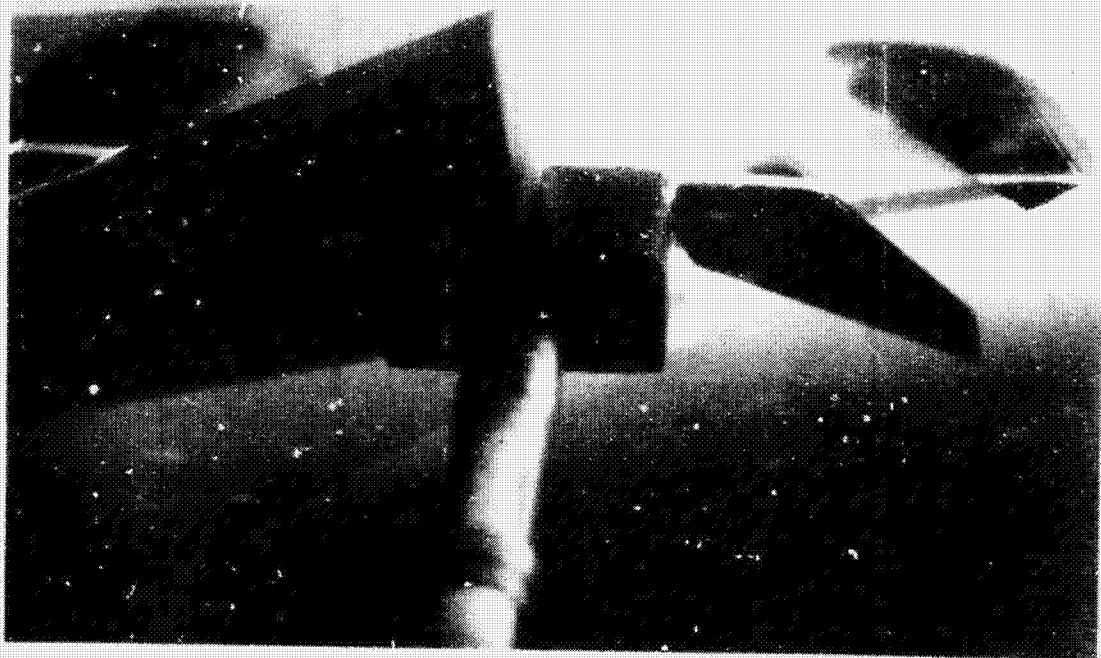
(5)





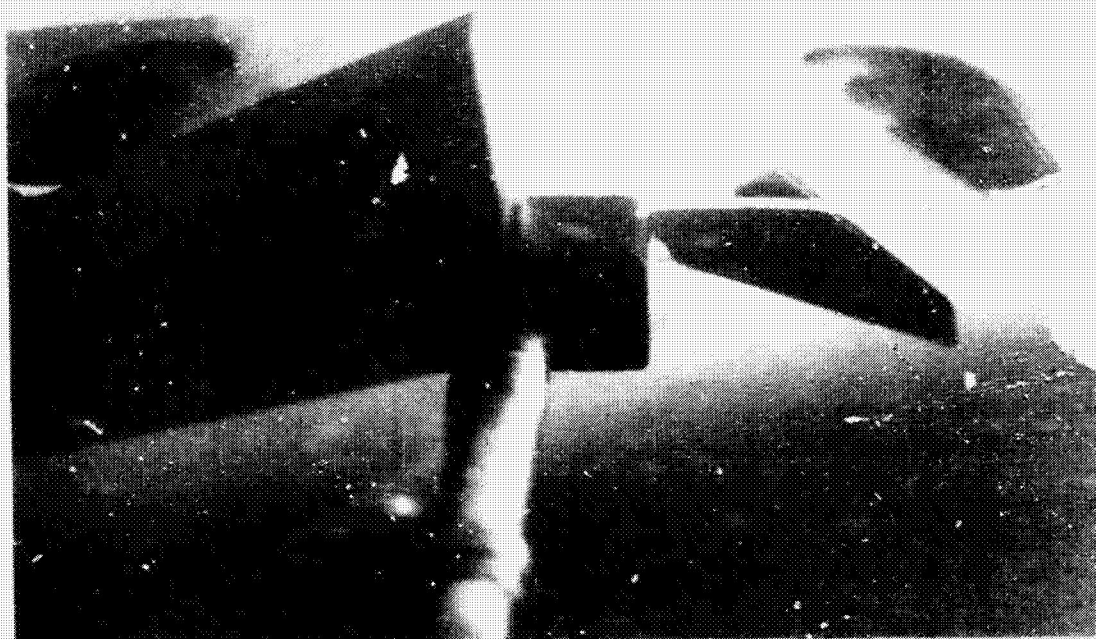
63

(6)



64

(7)



65

(8)

